

Transmission Electron Microscopy: a complement to X-rays and Neutrons

Amanda Petford-Long

Center for Nanoscale Materials, Argonne National Laboratory
Materials Science and Engineering Dept, Northwestern Univ.

What can we do with TEM??

Pulsed electron gun

Ion/particle sources

Monochromator

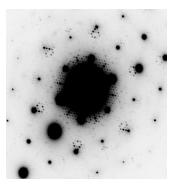
Aberration correction

Variable temperature

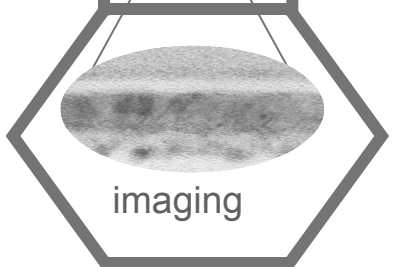
Need more than one instrument so that capabilities are not compromised
Design “electron optical beam lines” dedicated to specific applications

Energy filter

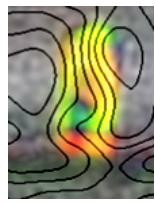
High speed detectors



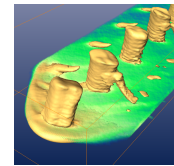
diffraction



imaging



holography



Tomography



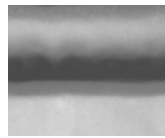
chemical map



Lorentz



spectroscopy



HAADF



Imaging and diffraction: 2D and 3D Structure

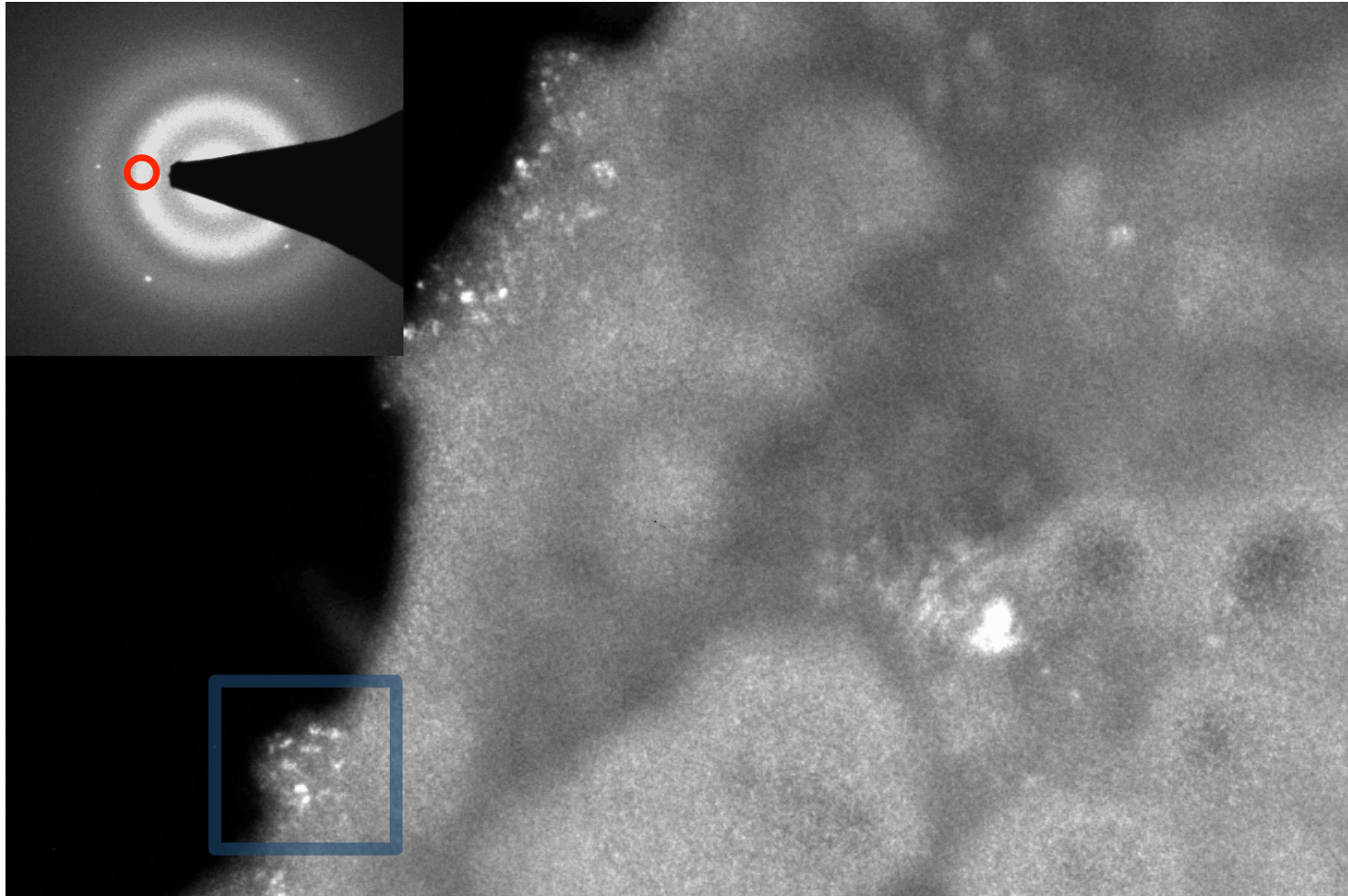


Origin of image contrast in TEM

- Mass contrast
 - Absorption differences for different materials
- Diffraction Contrast
 - Contrast depends critically on diffraction conditions
- Phase Contrast
 - Contrast depends on phase shift of electrons passing through sample
 - High resolution electron microscopy – weak phase object approximation
 - $\psi = e^{i\sigma V(r)} \approx 1 + i\sigma V(r)$
 - Lorentz microscopy
 - Electron Holography
- High-angle annular dark field (HAADF) imaging
 - Also known as scanning TEM (STEM) contrast
 - A function of atomic number



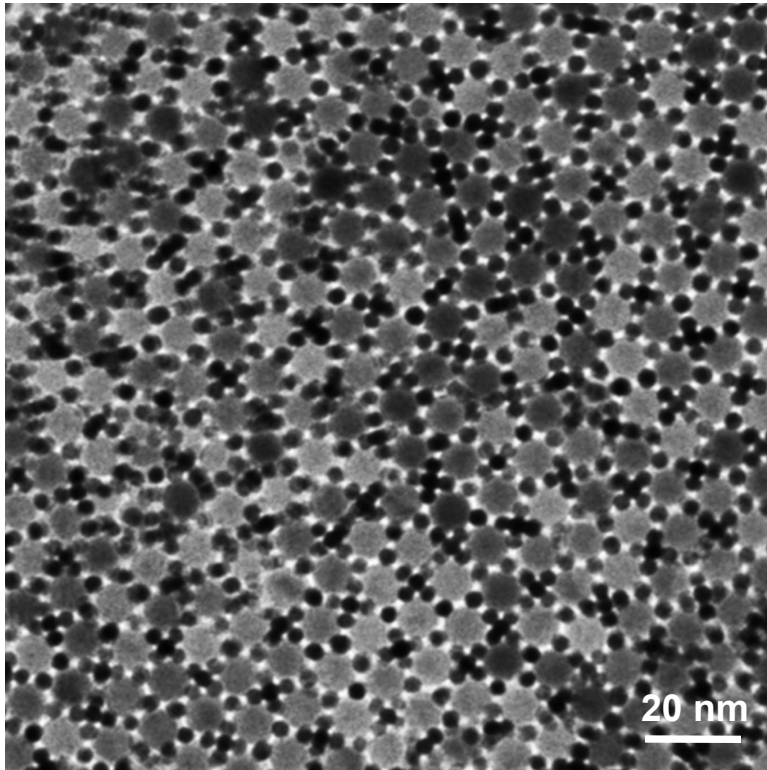
Partially-crystallized ZBLAN glass



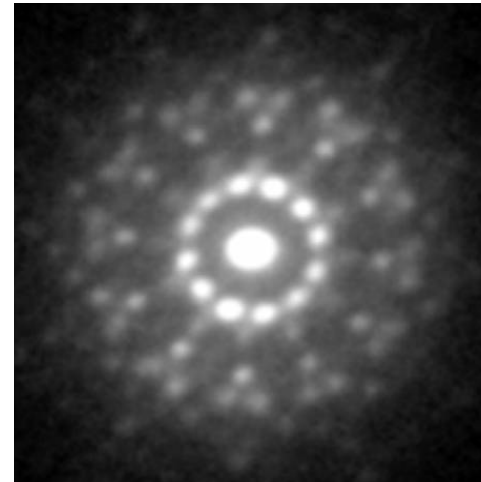
- Insert aperture to select defined region of the diffraction pattern. Contrast in image comes only from electrons diffracting within aperture



Au/Fe₃O₄ nanoparticle superlattice



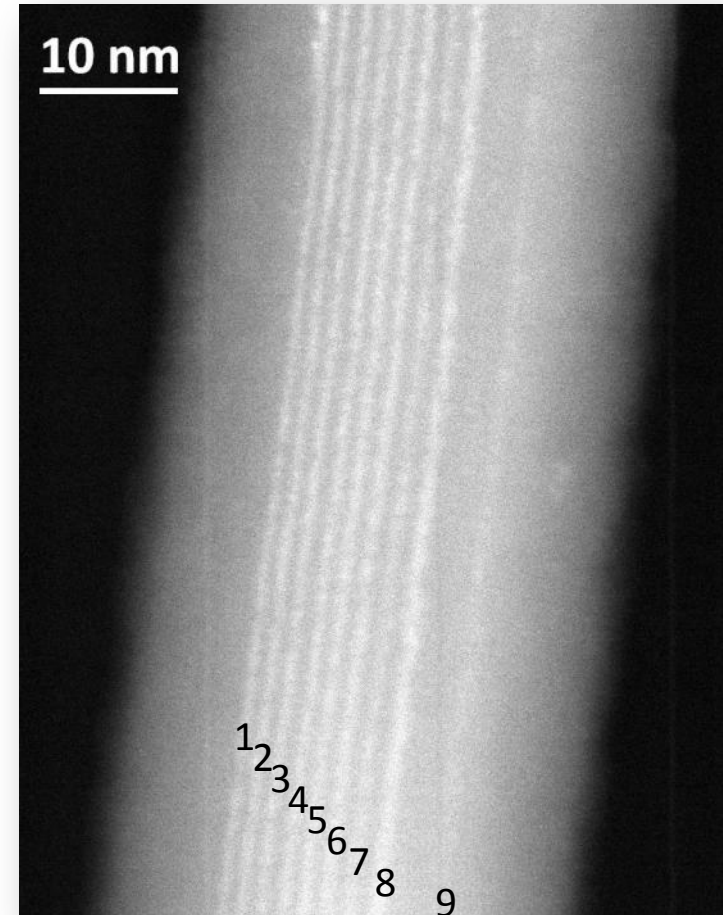
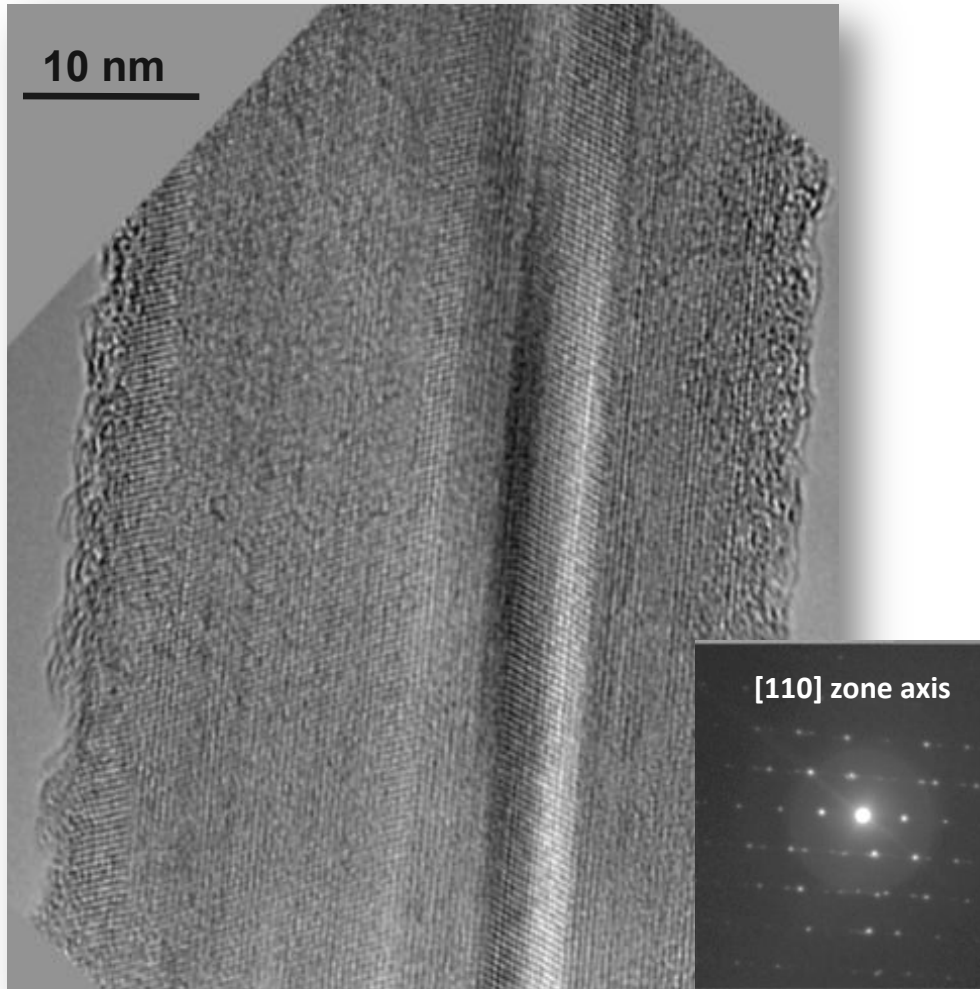
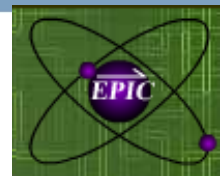
- Nanocrystals self-assemble to form quasicrystal structure



D.V. Talapin, E.V. Shevchenko, M. I. Bodnarchuk, X. C. Ye, J. Chen, and C.B. Murray, *Nature* **461**, 964 (2009).



Defective Si nanowire grown using Au catalyst

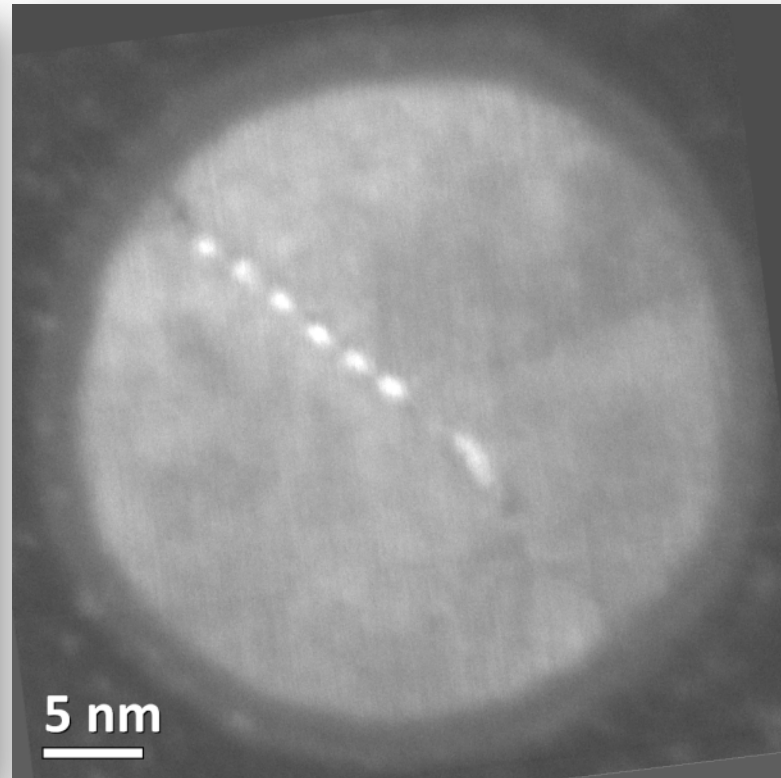
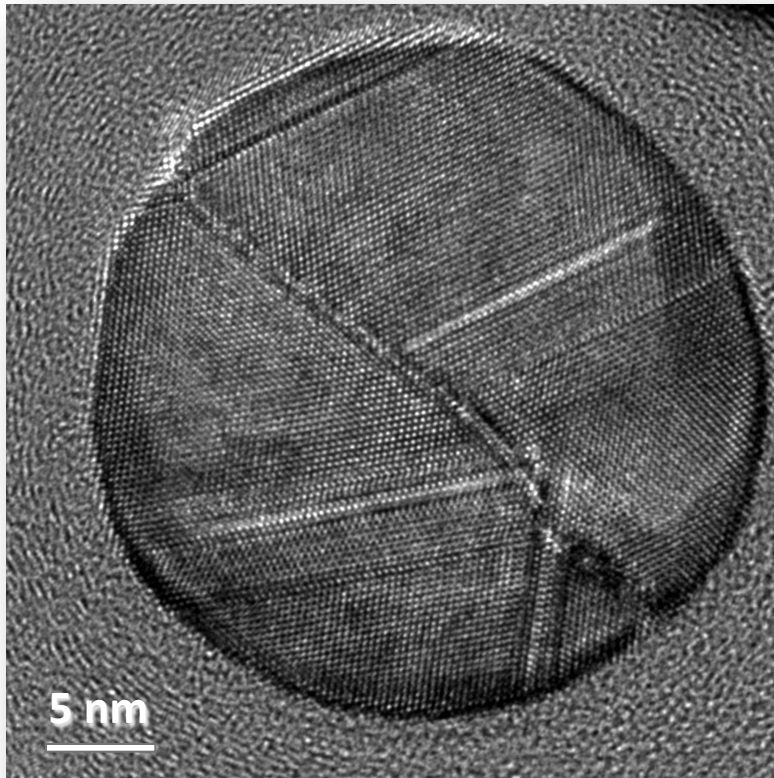
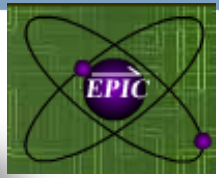


- Nanowire has a $[110]$ growth direction
- Nine lines of high atomic number atoms can be seen using HAADF
- Atomic lines appear with an ordered arrangement

Courtesy of E Hemesath and L Lauhon, Northwestern University.



Gold atoms at a grain boundary

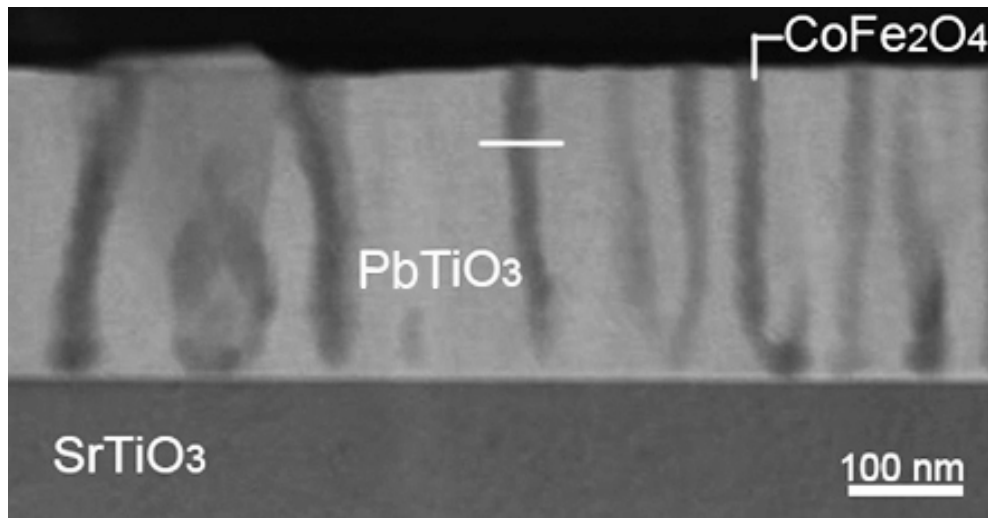


- Bicrystalline nanowire with an asymmetric $[110]$ tilt boundary
- $\sim 13^\circ$ misorientation
- Axial twin planes are present in both crystals
- Array of Au columns at the grain boundary

Courtesy of E Hemesath and L Lauhon, Northwestern University.
Cross-section sample prepared by D Schreiber and P Adusumilli

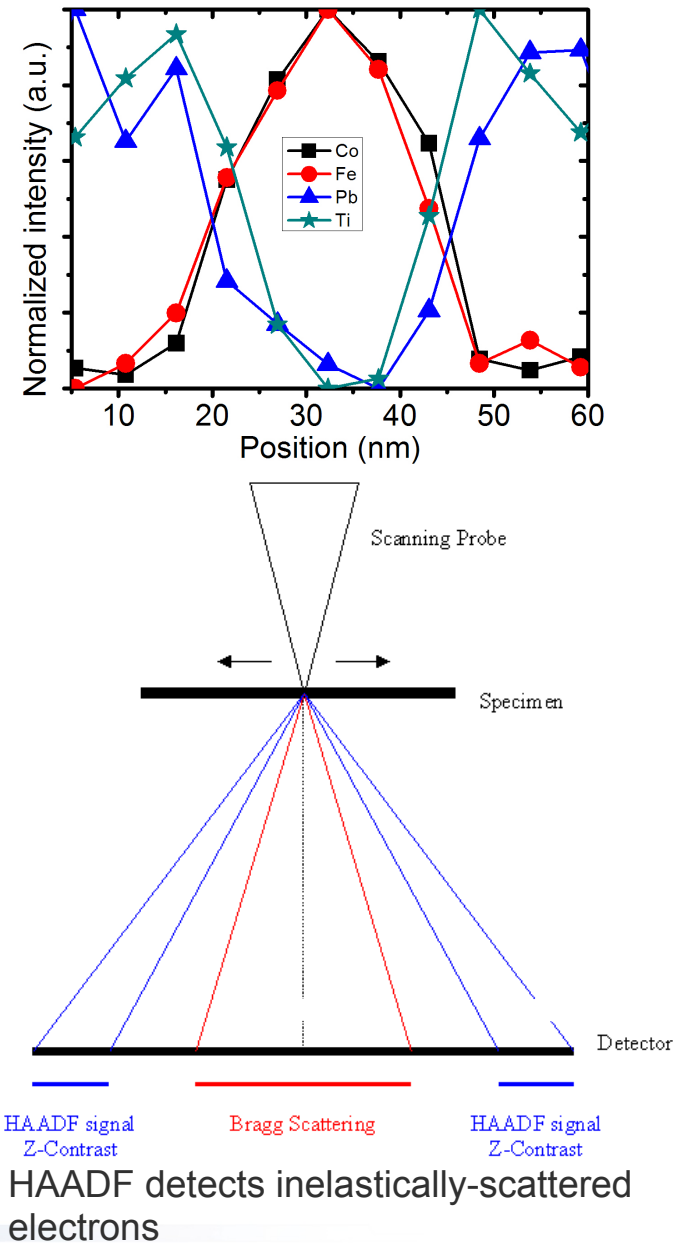


CoFe₂O₄/PbTiO₃ nanocomposite



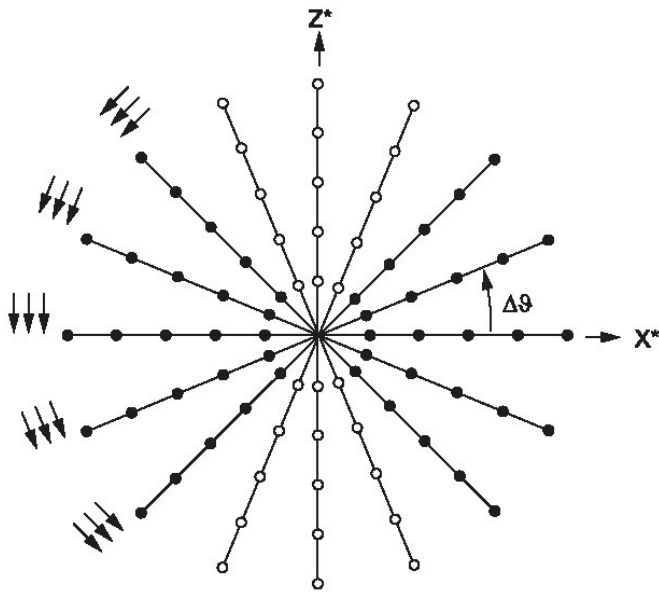
STEM HAADF image

Mengchun Pan, Yuzi Liu and Guoren Bai

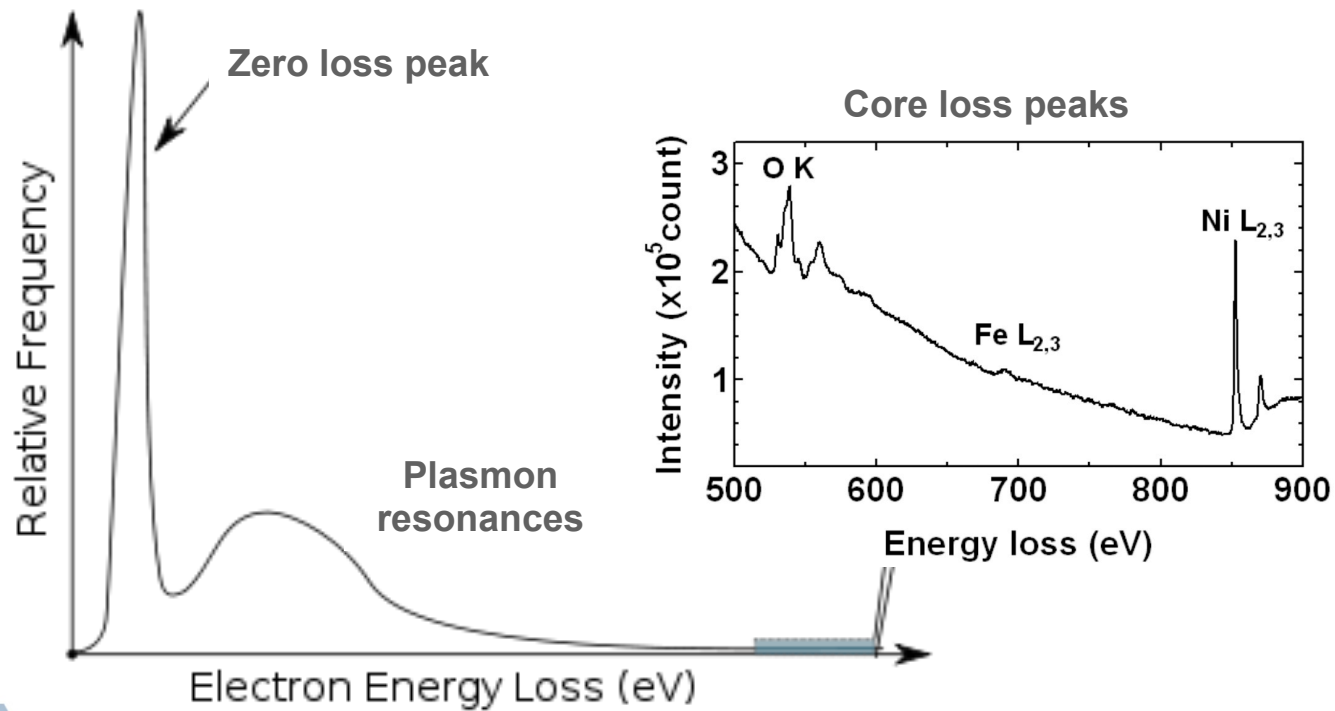


Electron tomography

- It is often the case that a two-dimensional view is not enough
- Three-dimensions is better!!
- Collect images over a large range of tilt angles
- Reconstruct using one of various methods to form 3D image of sample

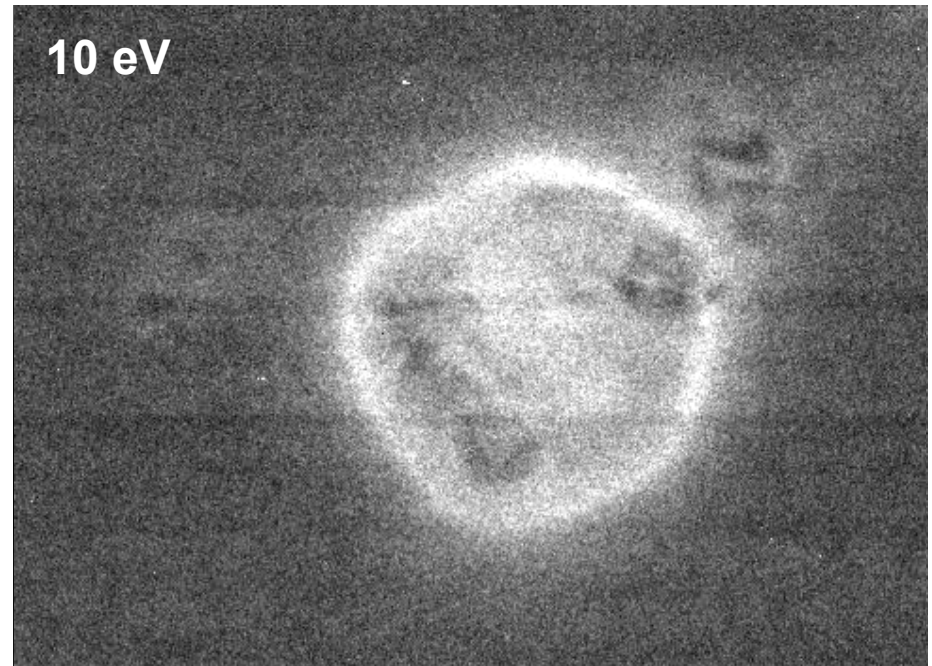
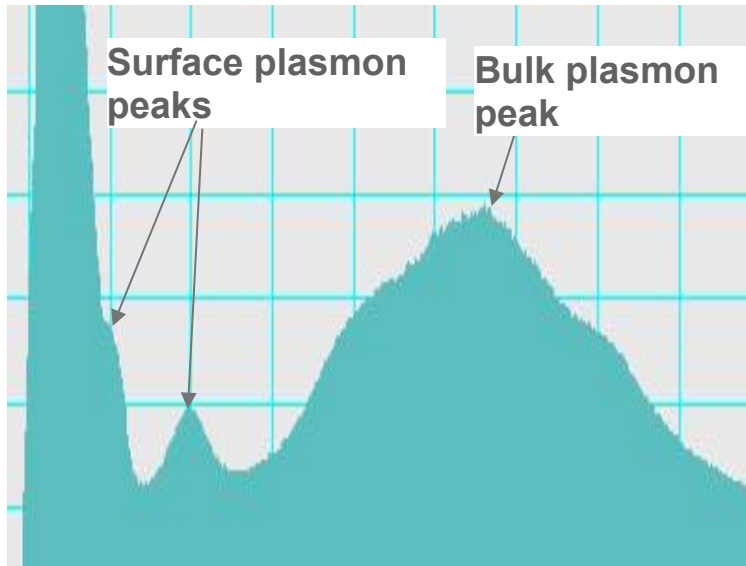


EELS and EFTEM



Core-shell nanoparticles

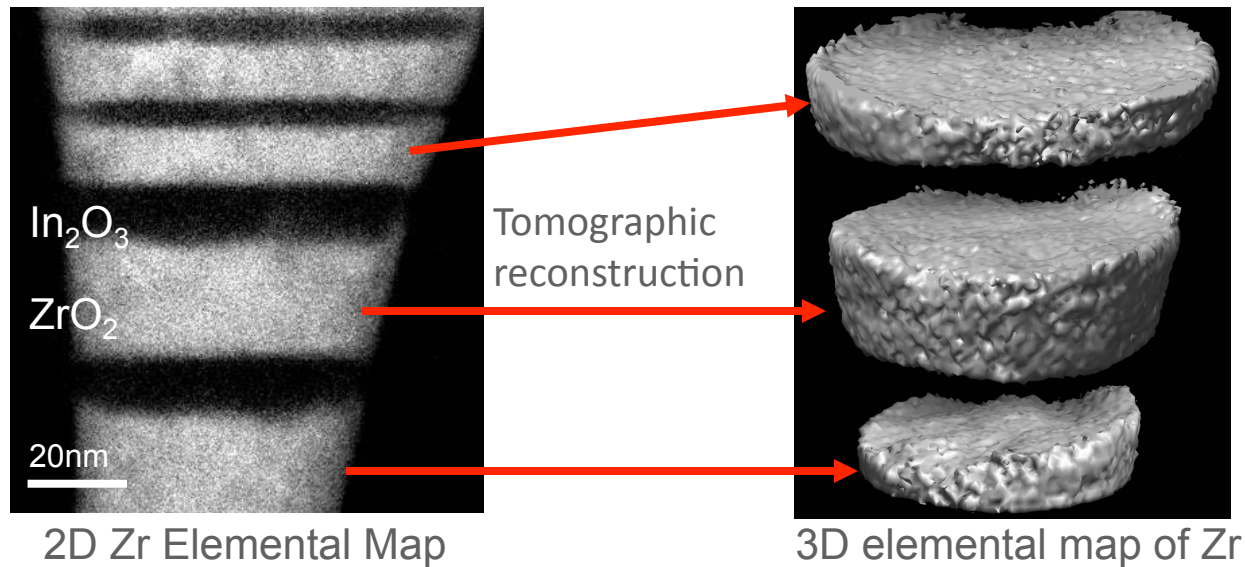
- 20 nm diameter Fe_3O_4 core with Ag shell
- Successive images are at energy loss shown on image
- Spatial extent of surface plasmon is clearly visible around Ag shell



Collaboration with Sara Majetich and Alex Eggeman,
Carnegie Mellon University

Interface structure of $\text{ZrO}_2/\text{In}_2\text{O}_3$ Multilayer Films

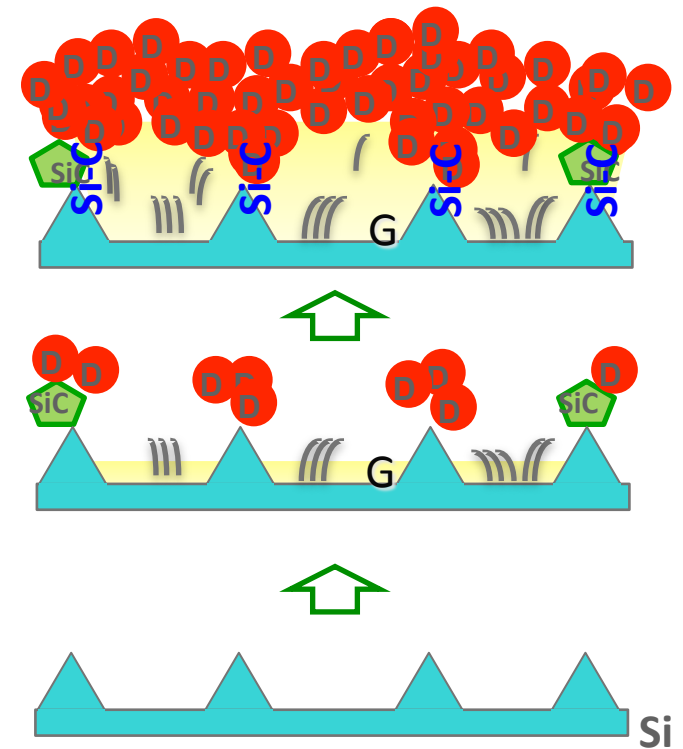
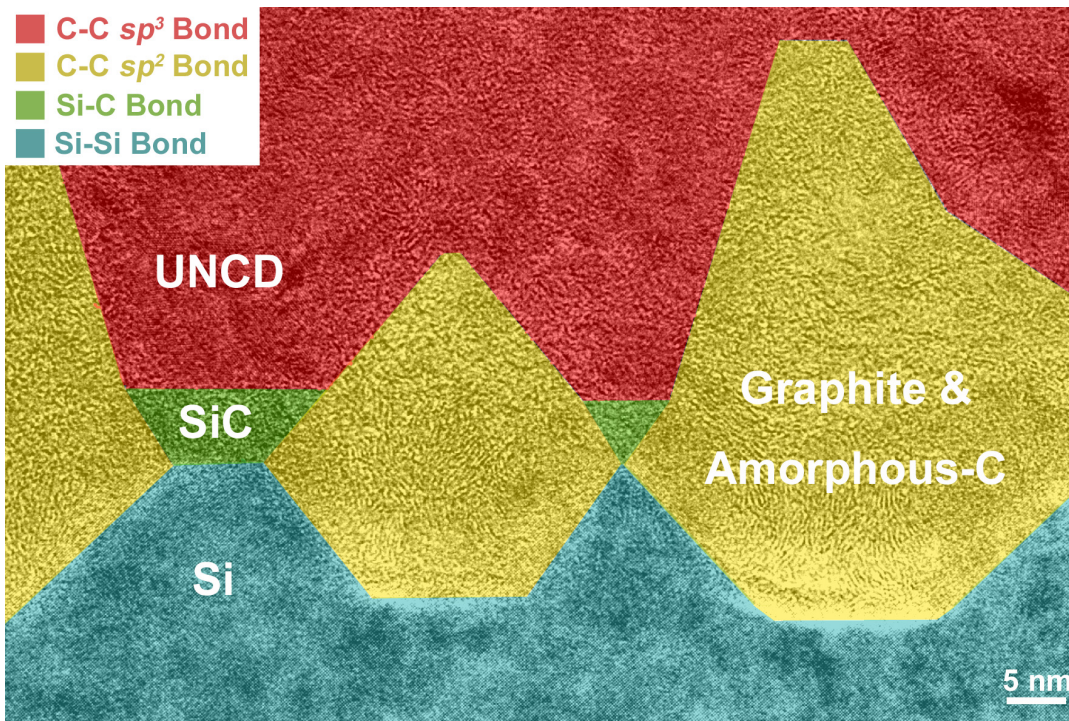
- 3D elemental map derived from energy-filtered images of an interface
- 3D characterization of the interfaces of a $\text{In}_2\text{O}_3 / \text{ZrO}_2$ multilayer
 - ZrO_2 on In_2O_3 : Rough interface on a nanometer scale
 - In_2O_3 on ZrO_2 : Sharp interface with a step of one unit cell



Xiaoyan Zhong, Bernd Kabius, Jeff Eastman, Dillon Fong

Nucleation of ultrananocrystalline diamond films on Si

◆ EFTEM mapping using C K edge identified inhomogeneous distribution of graphite, amorphous C and SiC at ultrananocrystalline diamond (UNCD)/Si interfaces and led to proposed mechanism for nucleation of UNCD films on Si



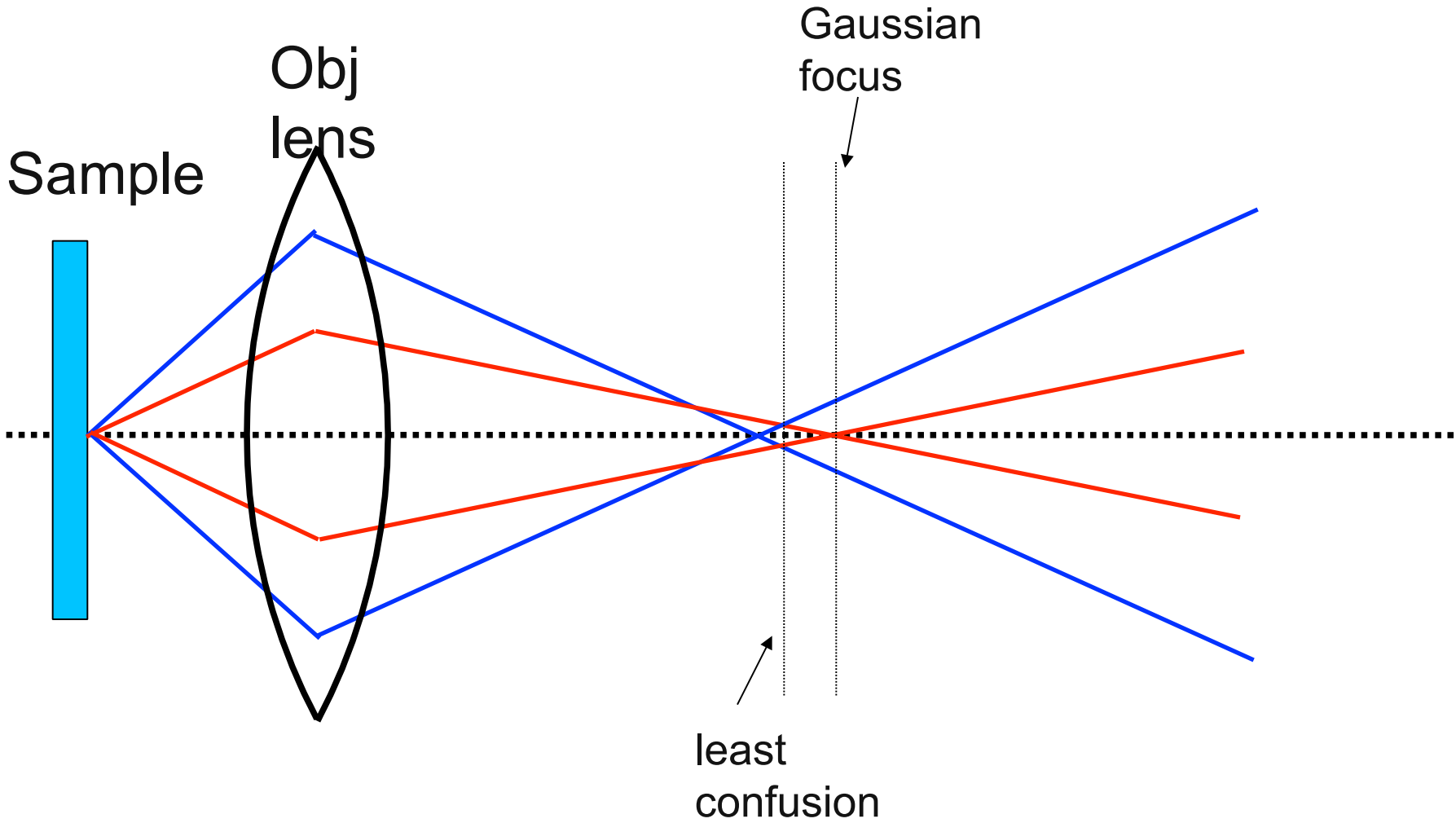
Xiaoyan Zhong, Bernd Kabius,

Y.C. Chen, X. Y. Zhong et al.
Appl. Phys. Lett. 92, 133113 (2008)

Aberration-correction



Spherical Aberration: C_s

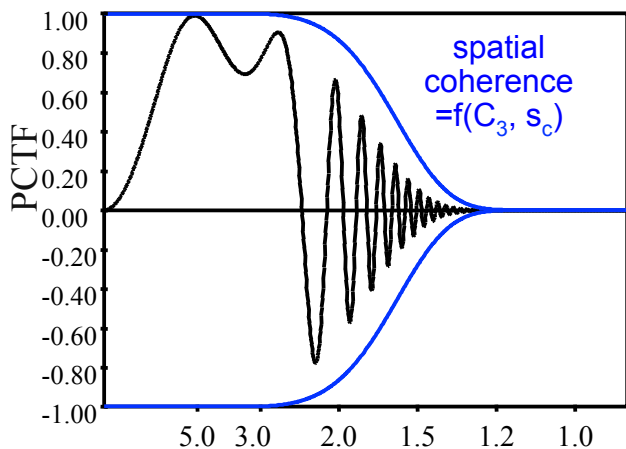


Slide courtesy of Bernd Kabius

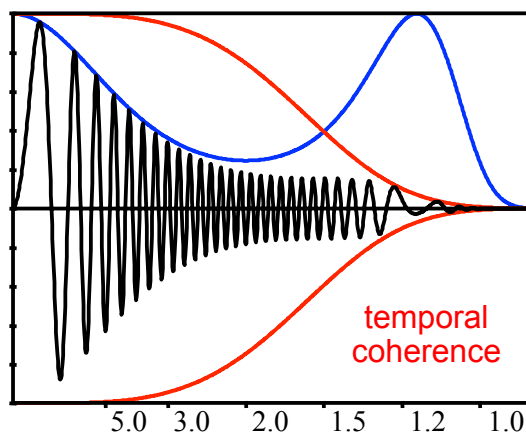


C_s correction

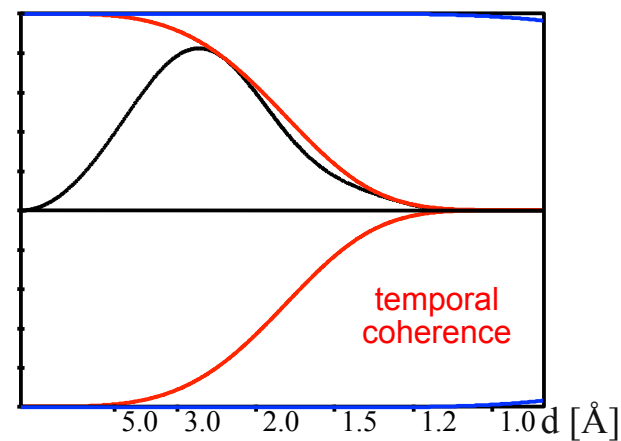
Scherzer



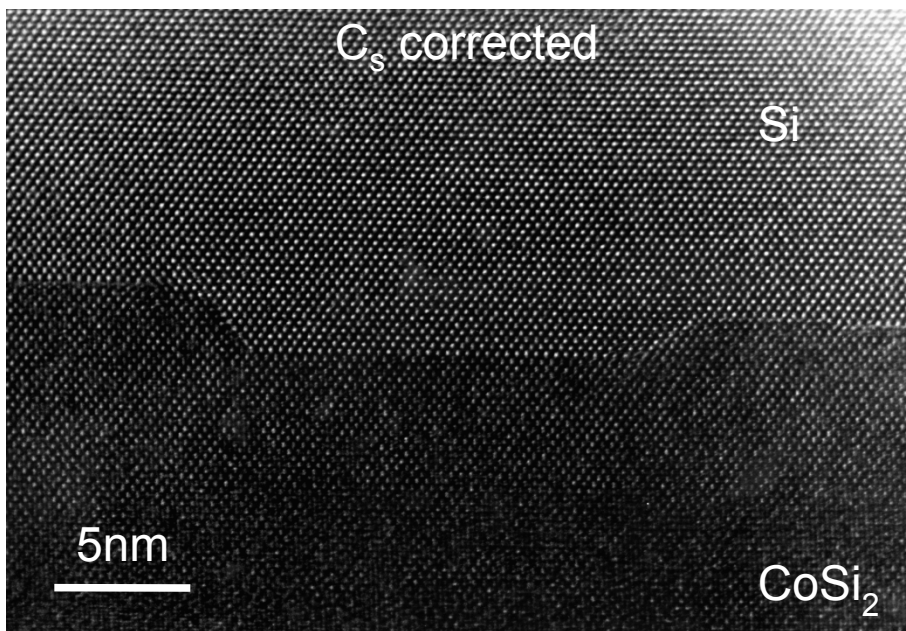
least confusion



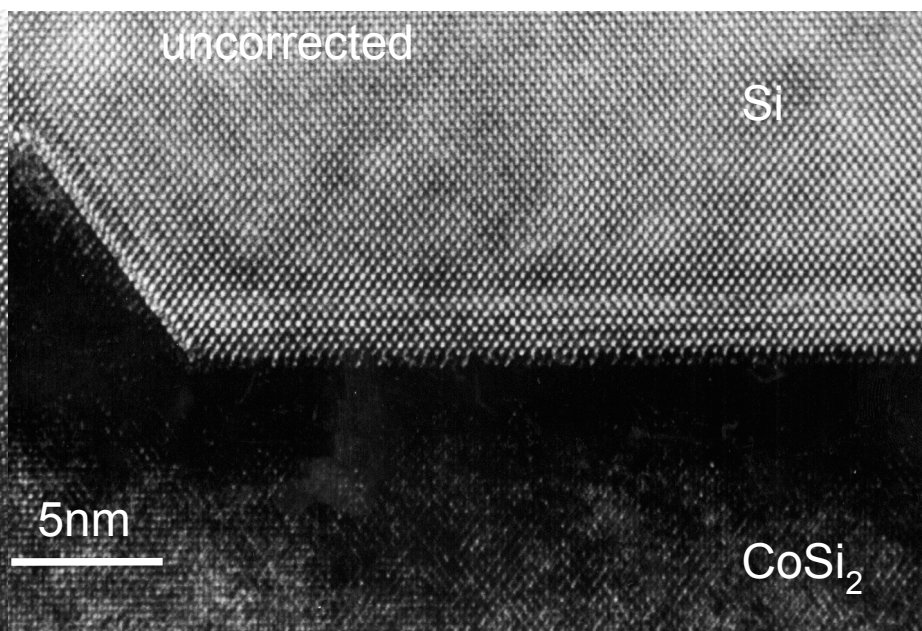
C_s corrected



C_s corrected



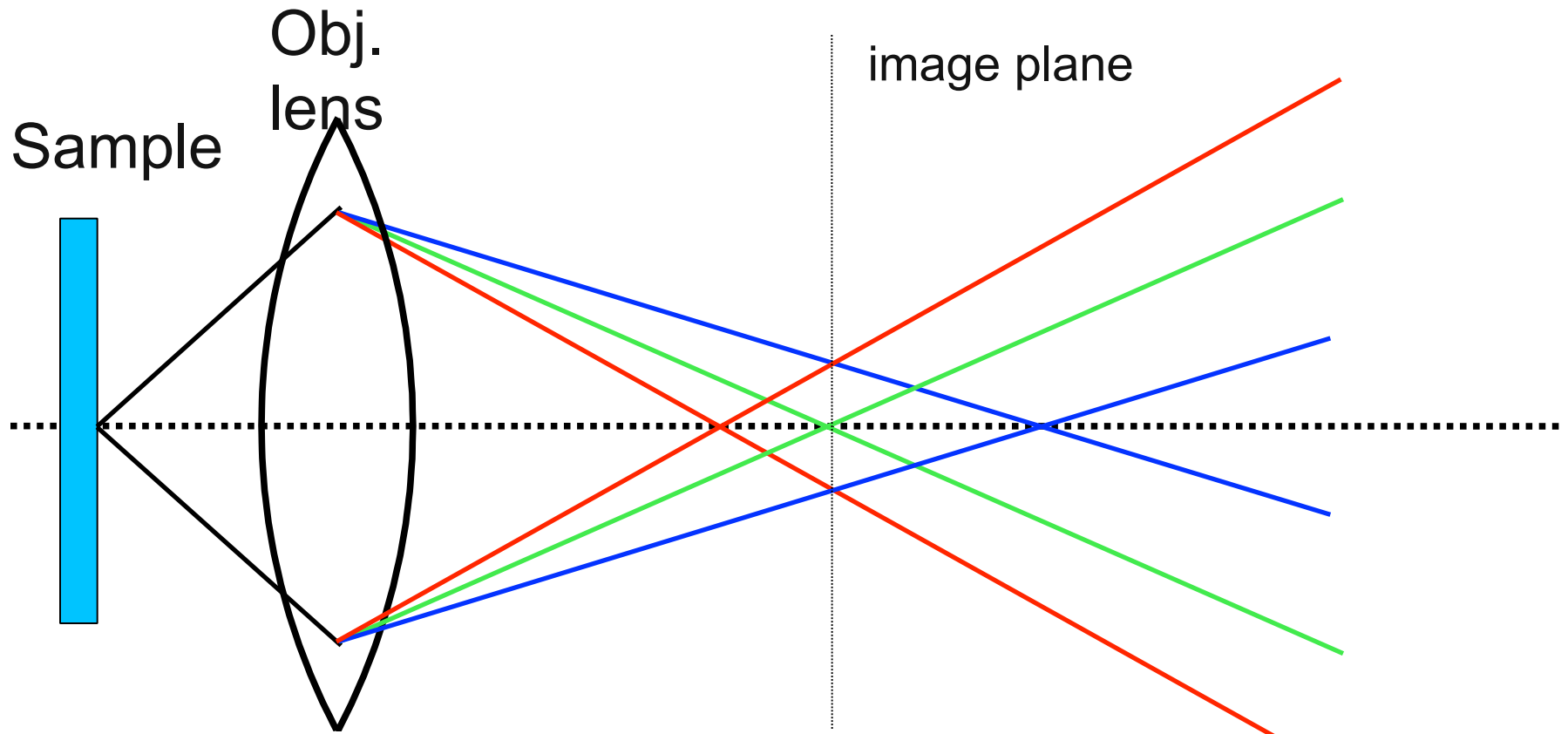
uncorrected



Slide courtesy of Bernd Kabius



Chromatic aberration: C_c

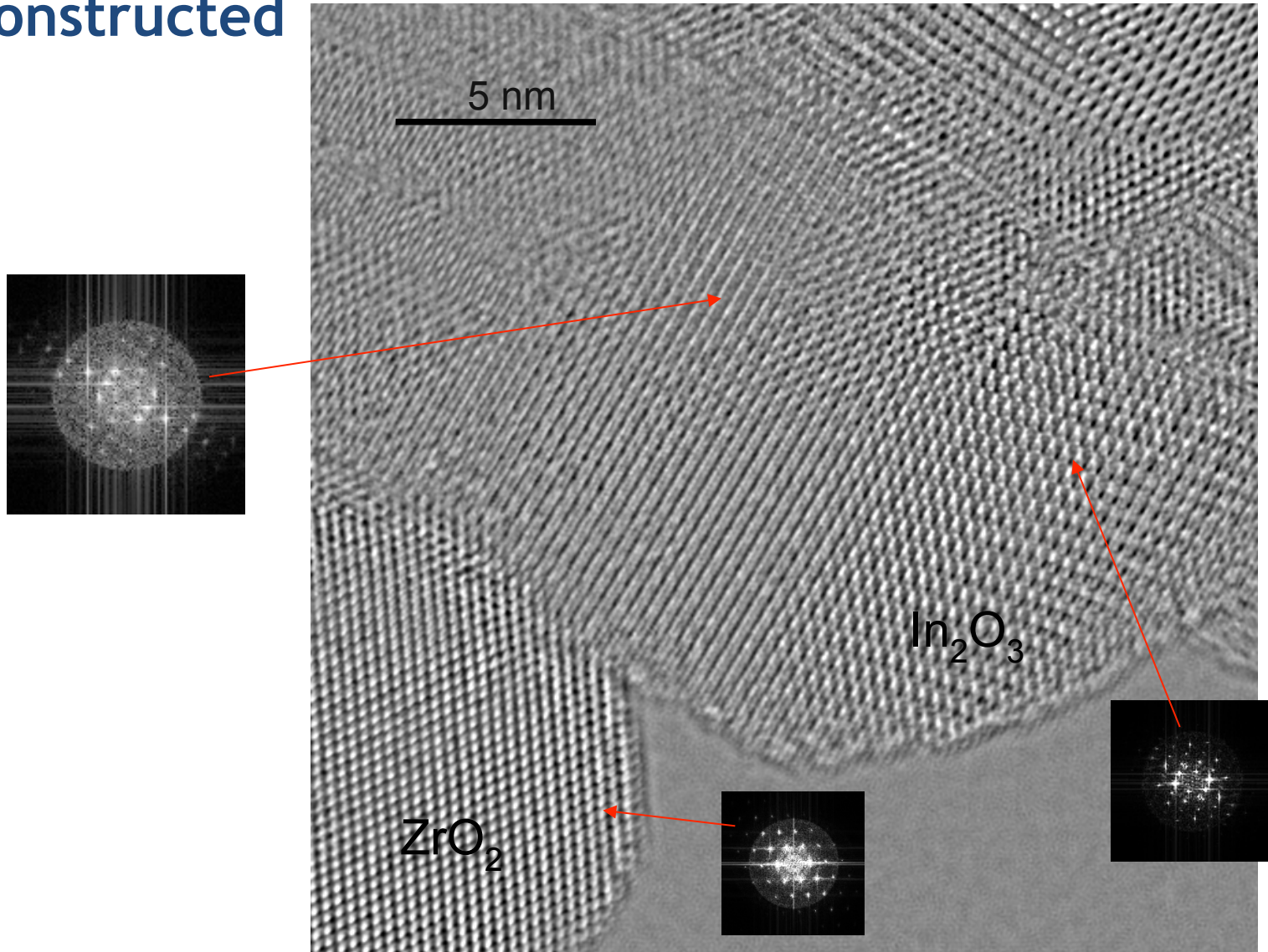


$$E_t = \exp \left[\frac{-(0.5 \pi \lambda d_s)^2 * q^4}{1.0 + (\pi \lambda s_c d_s)^2} \right]$$

$$d_s = \sqrt{\left(d_s^{\mathcal{Q}} \frac{2 \Delta I_{\mathcal{Q}}}{I_{\mathcal{Q}}} \right)^2 + \left(d_E^{\mathcal{Q}} \frac{\Delta E_{\mathcal{Q}}}{E_{\mathcal{Q}}} \right)^2 + \left(C_c \sqrt{\left(\frac{\Delta E}{E} \right)^2 + \left(\frac{\Delta H}{H} \right)^2 + \left(\frac{2 \Delta I}{I} \right)^2} \right)^2}$$

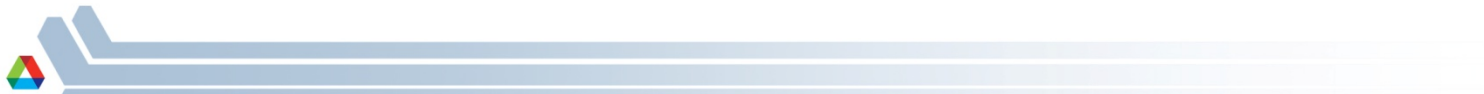
Slide courtesy of Bernd Kabius

ZrO₂ / In₂O₃ on YSZ: C_c corrected, 80kV Phase reconstructed



Slide courtesy of Bernd Kabius

Imaging Electric and Magnetic Fields

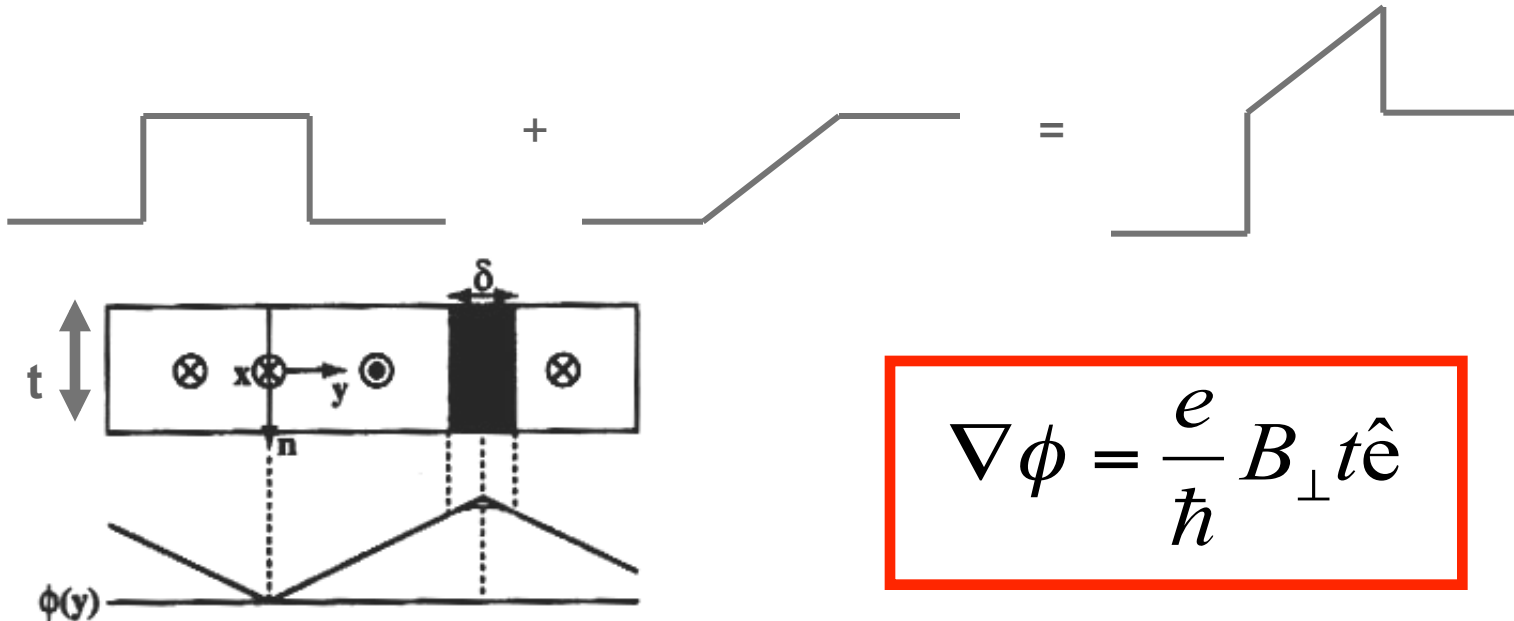


Making use of phase shift to image fields

The phase ϕ of an electron wave (wavelength λ) is modified when passing through a sample in the presence of electromagnetic potentials V and A ($B = \nabla \times A$)

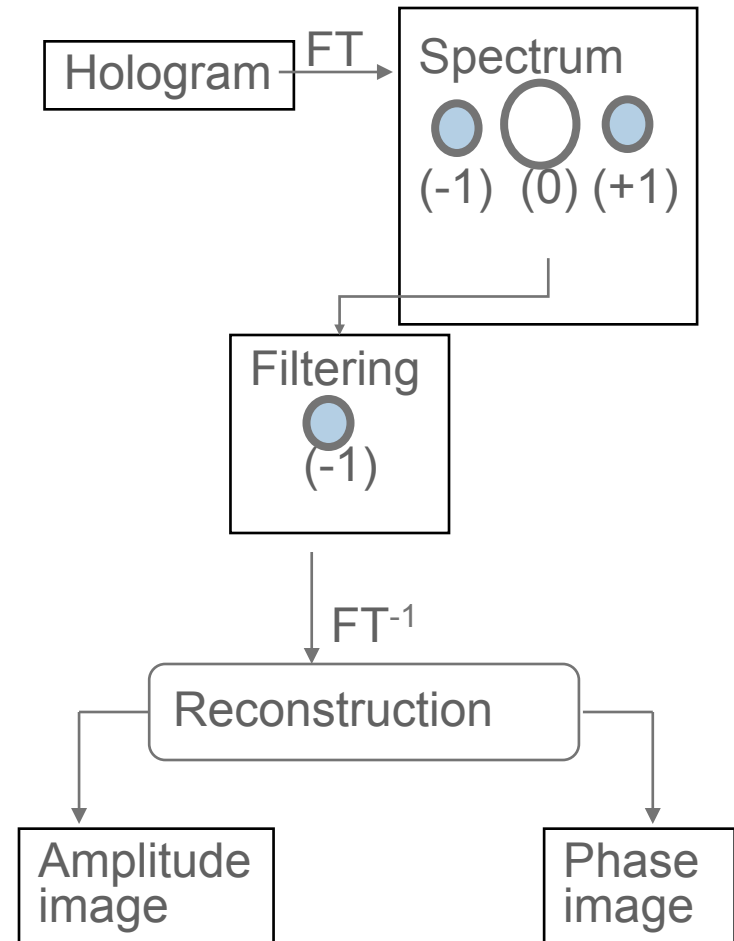
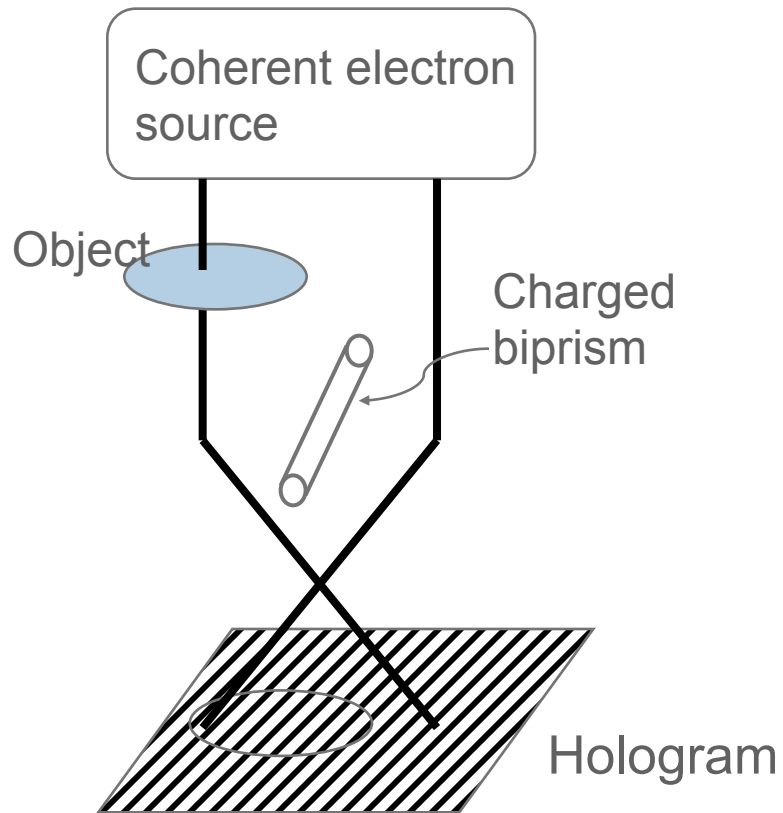
$$\phi = \frac{\pi}{\lambda E_t} \int_L V(r_{\perp}, z) dz - \frac{e}{\hbar} \int_L A(r_{\perp}, z) dz$$

E_t – total energy of the beam electrons; z – coordinate along the optic axis;
 r_{\perp} – radial coordinate in the sample plane



$$\nabla \phi = \frac{e}{\hbar} B_{\perp} t \hat{e}$$

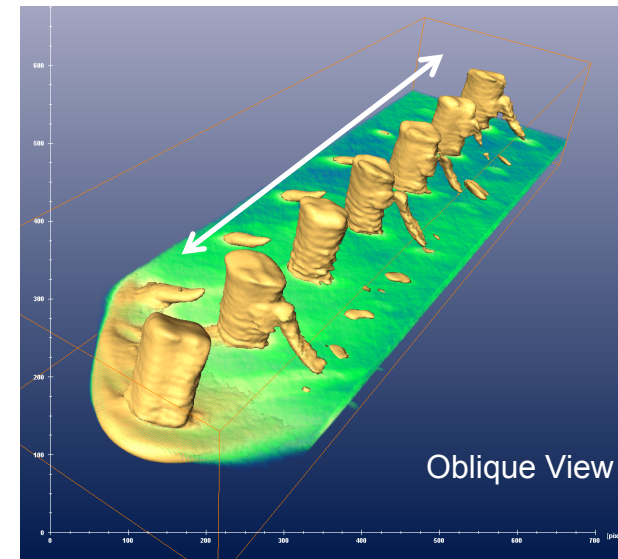
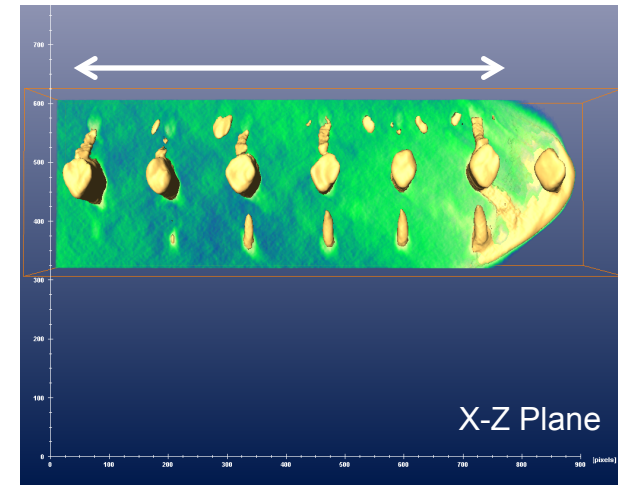
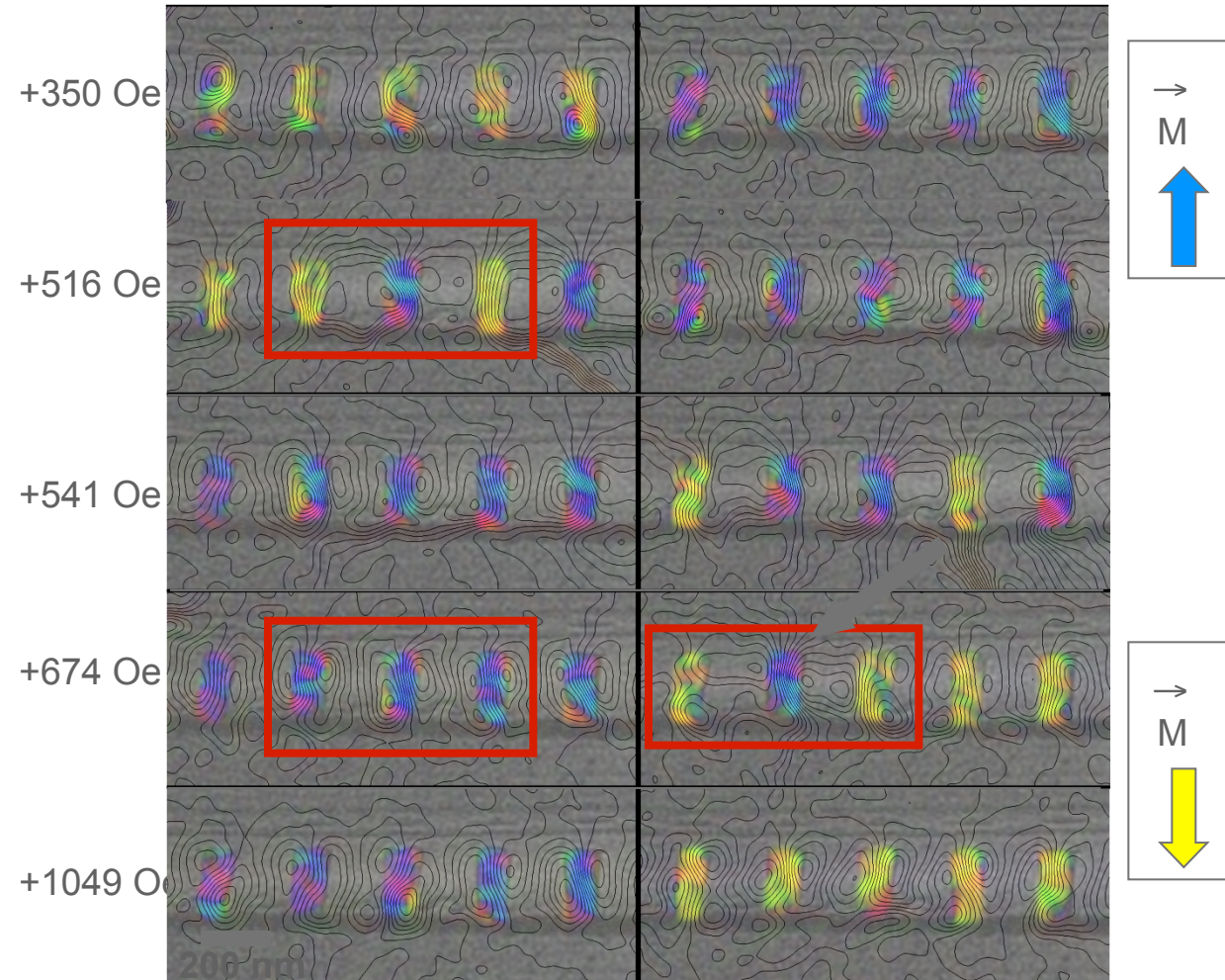
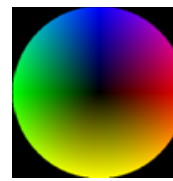
Electron holography



- adjacent interference fringes are separated by a flux quantum, h/e
- Images are non-trivial to interpret

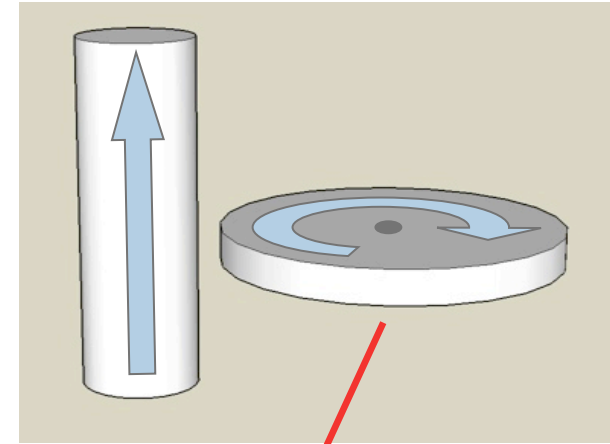
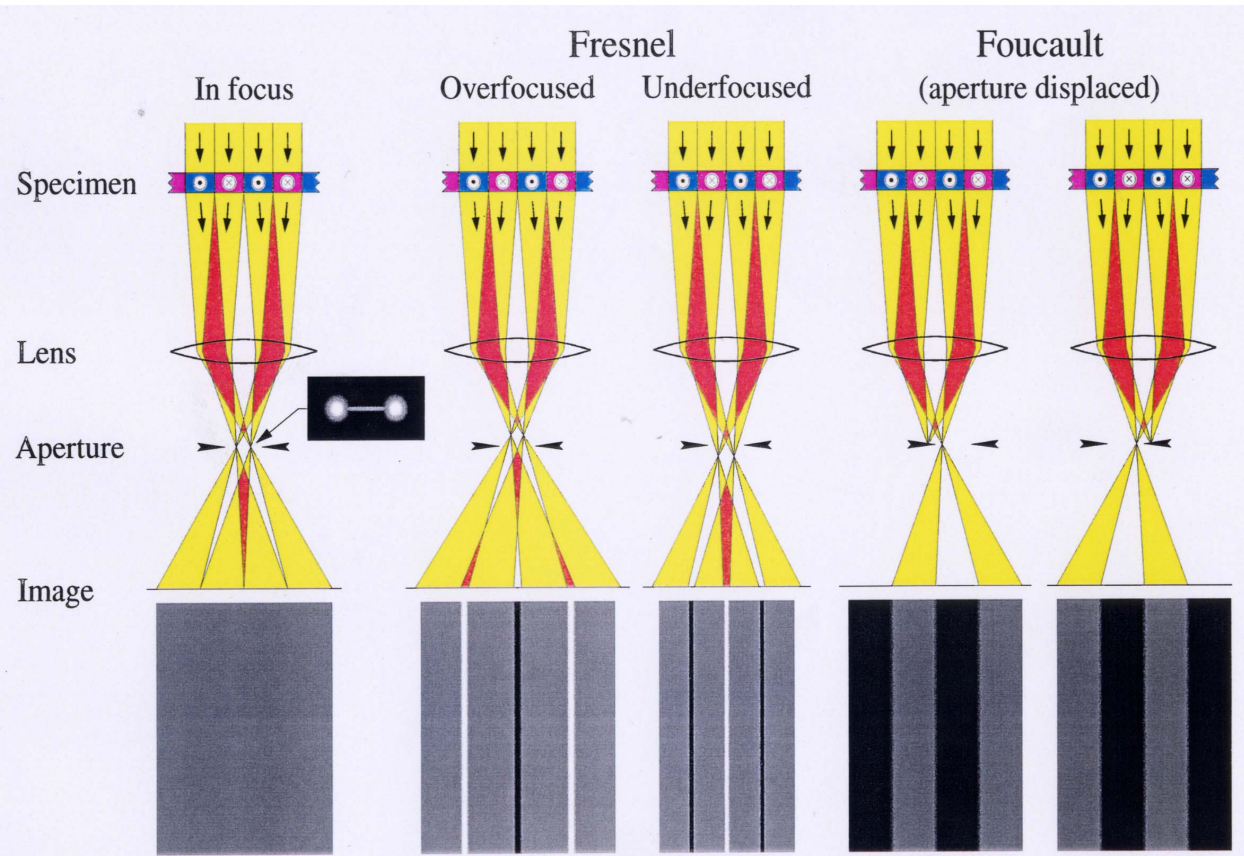


Ni pillars

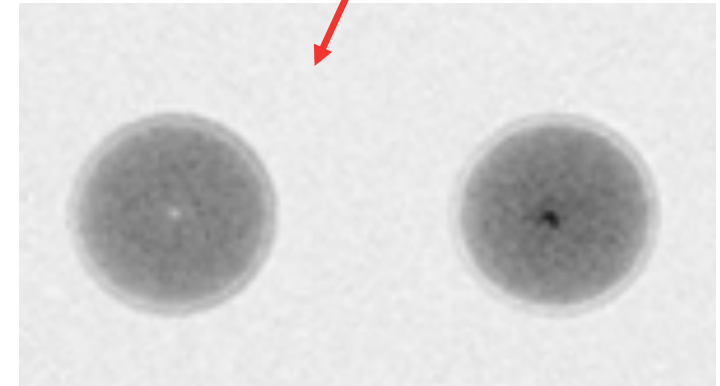


Remanent state magnetic induction maps for Ni pillars after application of different applied fields

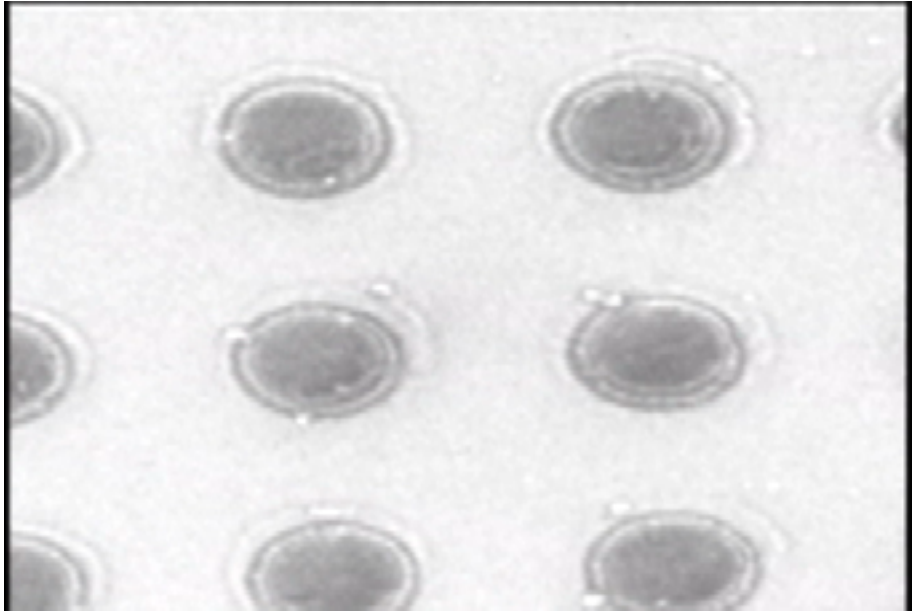
Lorentz TEM



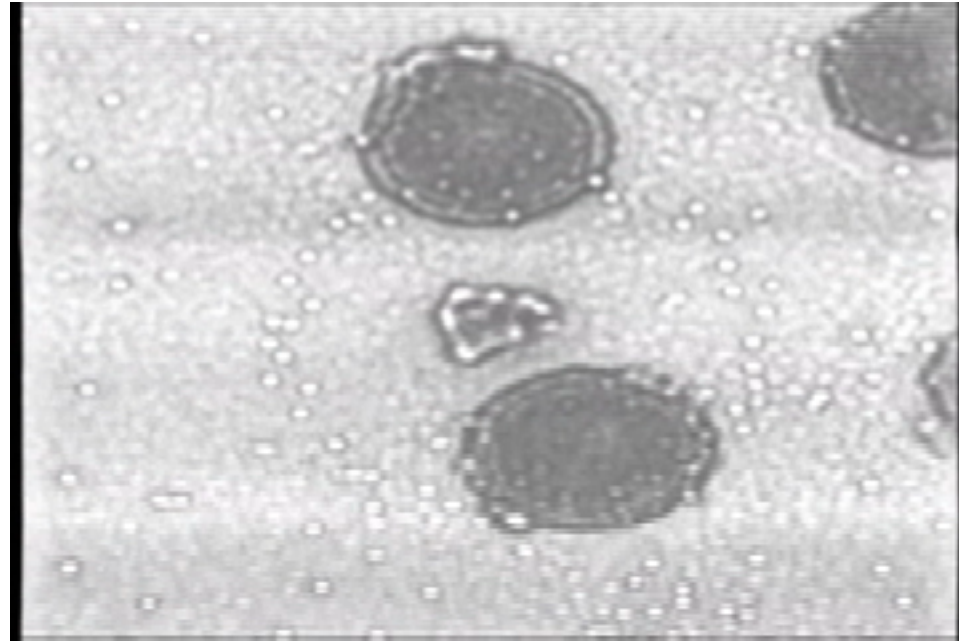
- Field applied in-situ:
 - Using magnetizing coils in a sample holder
 - By tilting sample into lens field
- Time resolution not good: can image time-averaged behavior



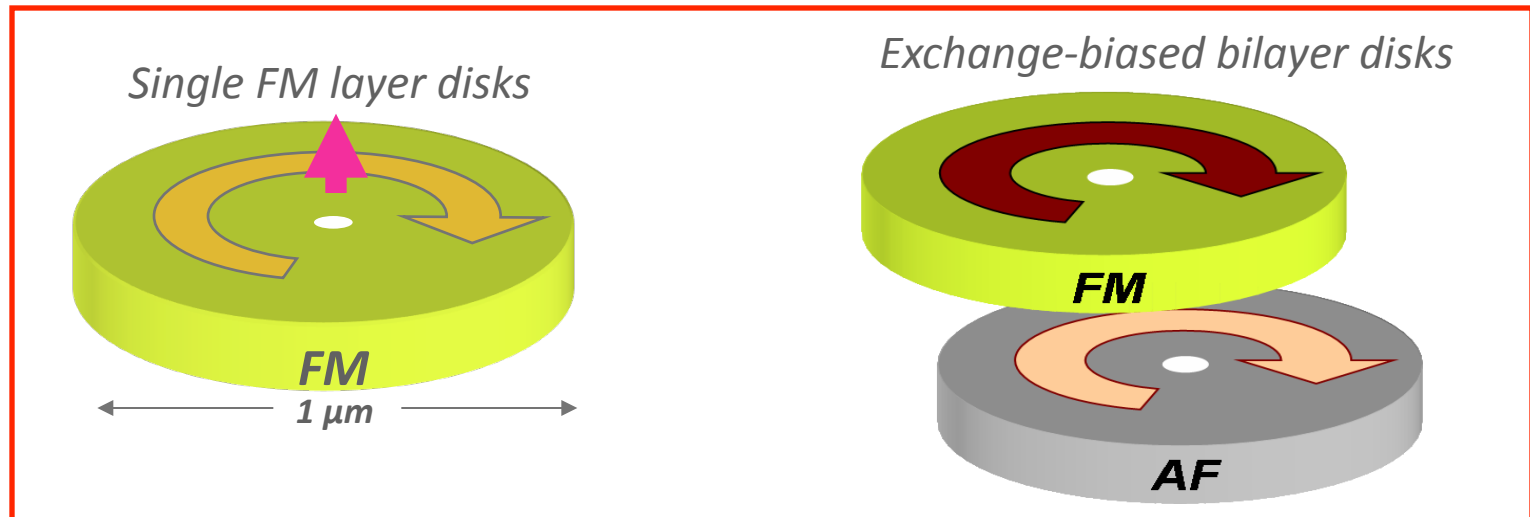
Reversal mechanisms in NiFe and NiFe/IrMn disks



Single layer NiFe disk



Bilayer NiFe/IrMn disk



Single FM layer disks

Exchange-biased bilayer disks

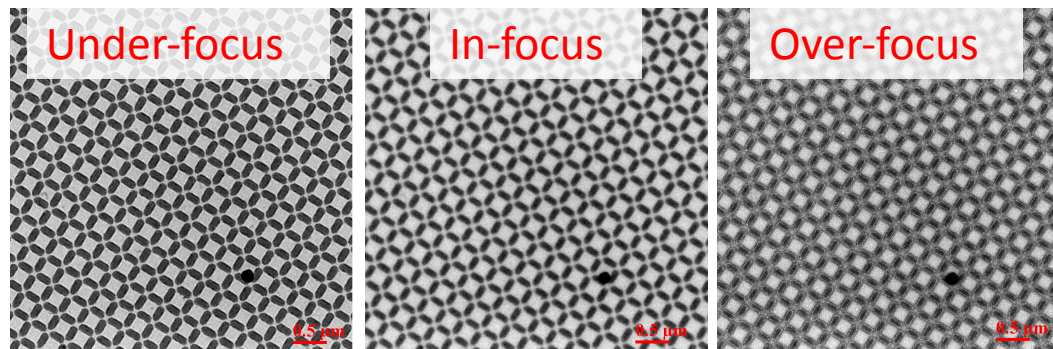
FM

1 μm

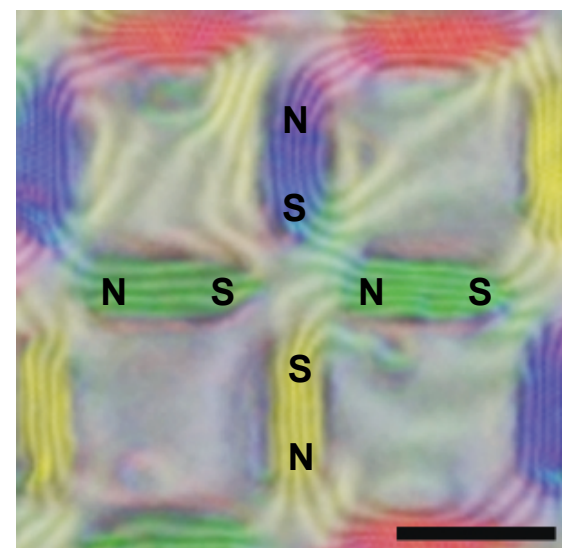
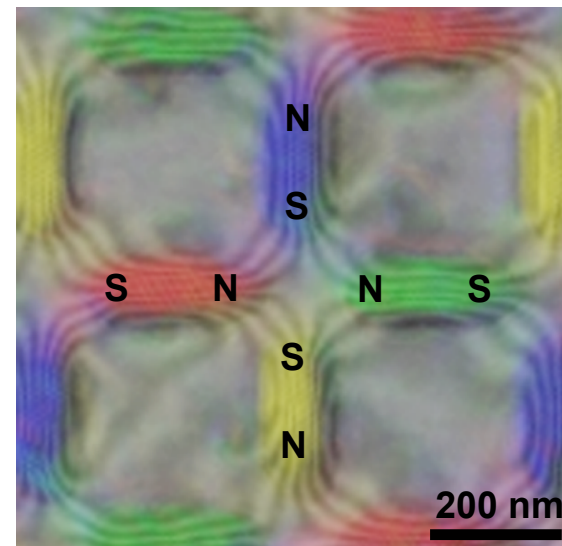
FM

AF

Spin ice structure



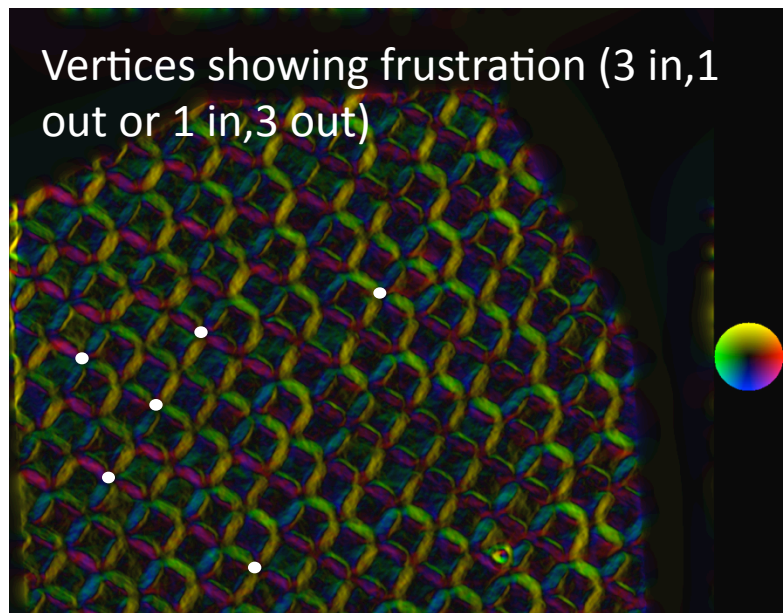
Array of NiFe stadia: 200 nm long



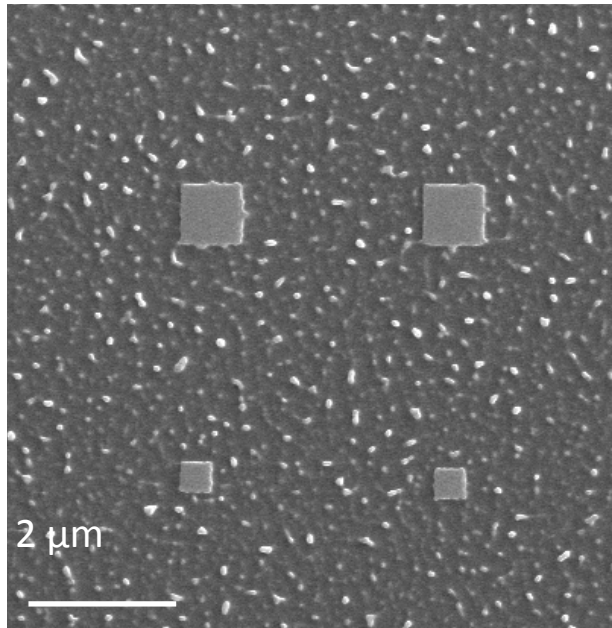
Images showing standard vertex obeying spin ice rule (L) and vertex showing emergent magnetic monopole (R)

“Transport of Intensity” equation

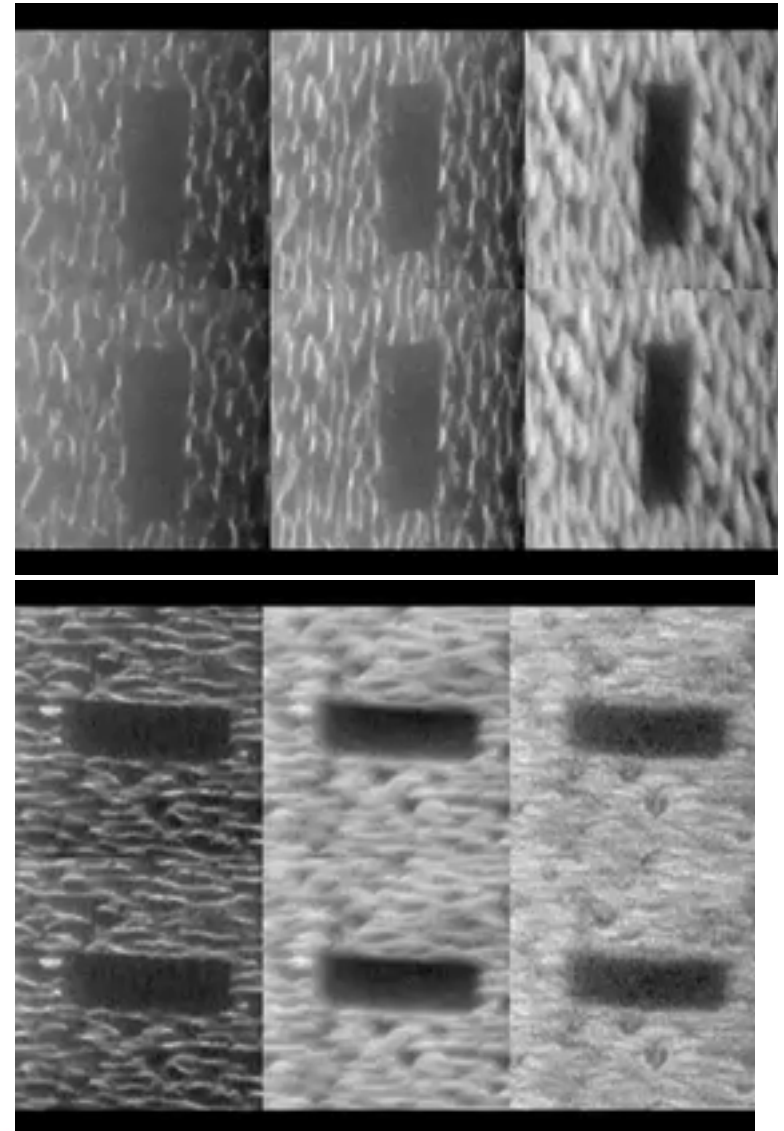
$$\nabla_{\perp} \cdot [I(r_{\perp}, z) \nabla_{\perp} \phi(r_{\perp}, z)] = -k \partial_z I(r_{\perp}, z)$$



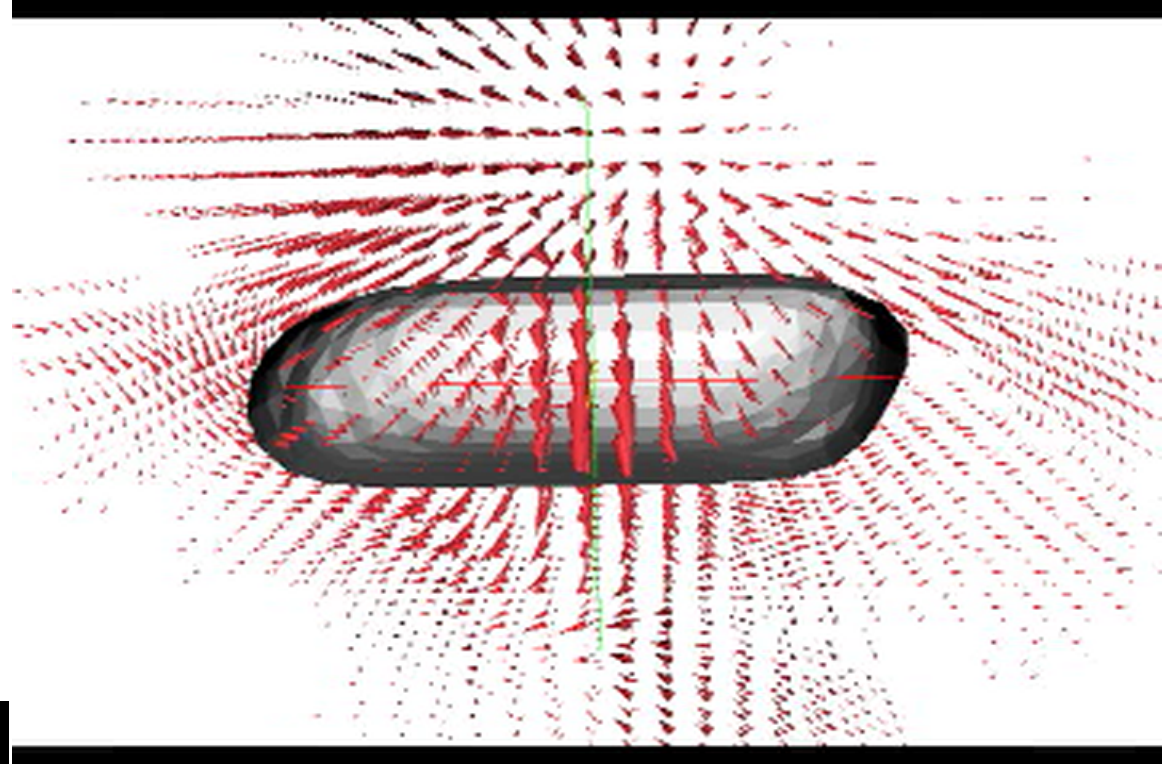
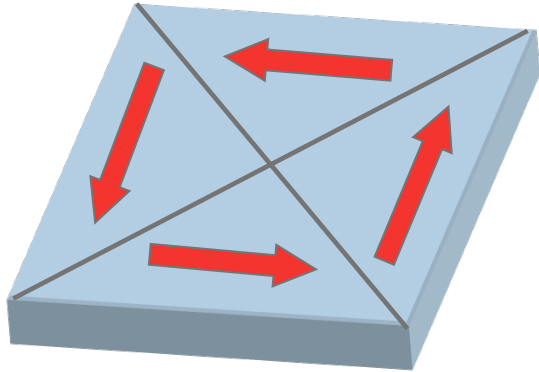
Vector field tomography of Permalloy square



- Structures patterned using direct FIB milling of Cr/Ni₈₀Fe₂₀ film deposited on SiO membrane
- Record four tomography tilt series, with three images at each angle
 - x; x/flipped; y; y/flipped



Scalar and vector tomography reconstructions



- Use Transport of Intensity Equation formalism to reconstruct scalar and magnetic vector potentials

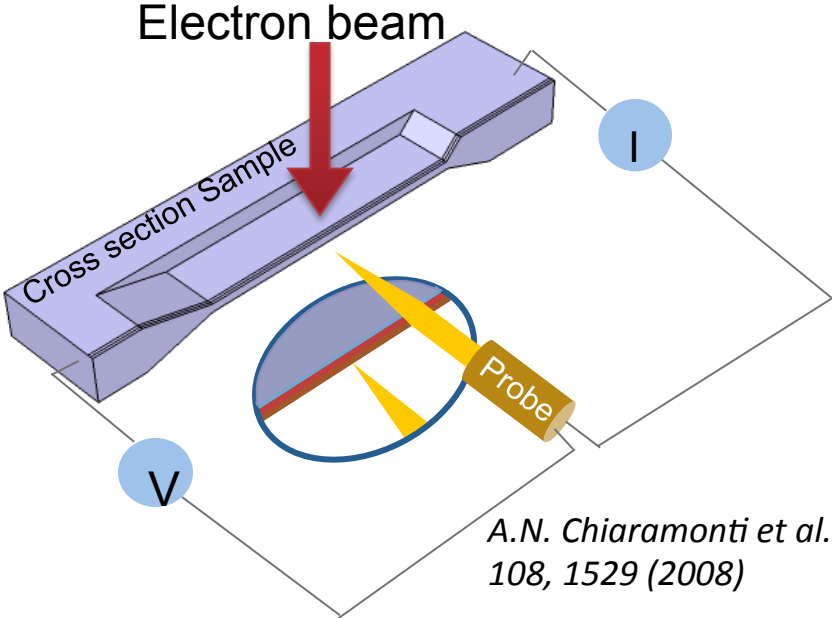
C D Phatak, A K Petford-Long and M De Graef,
PRL **104**, 253901 (2010).



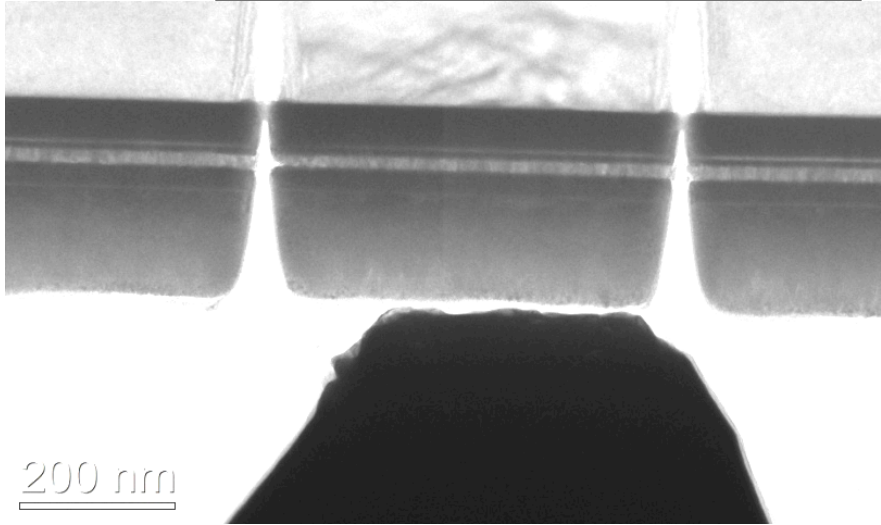
Measuring local transport behavior



Local Transport Behavior

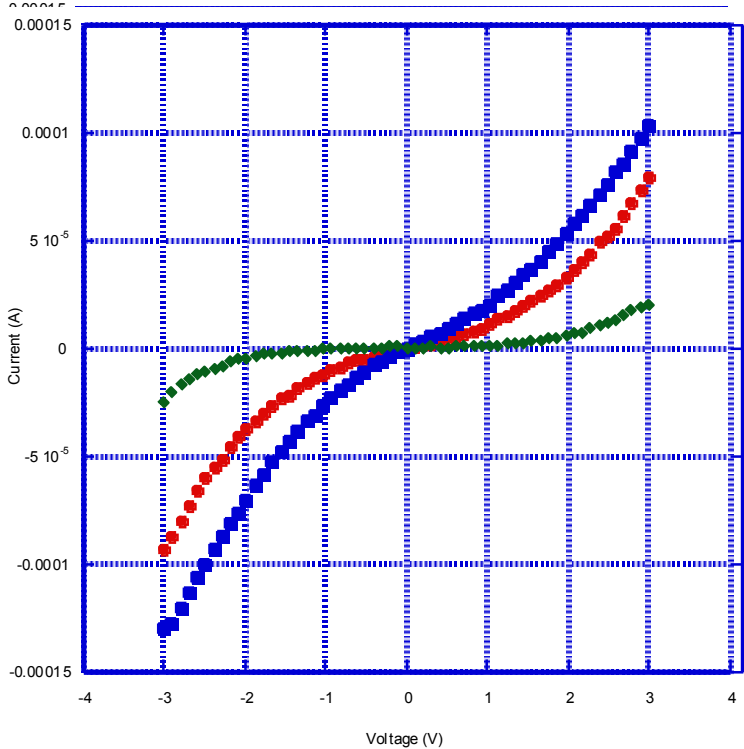
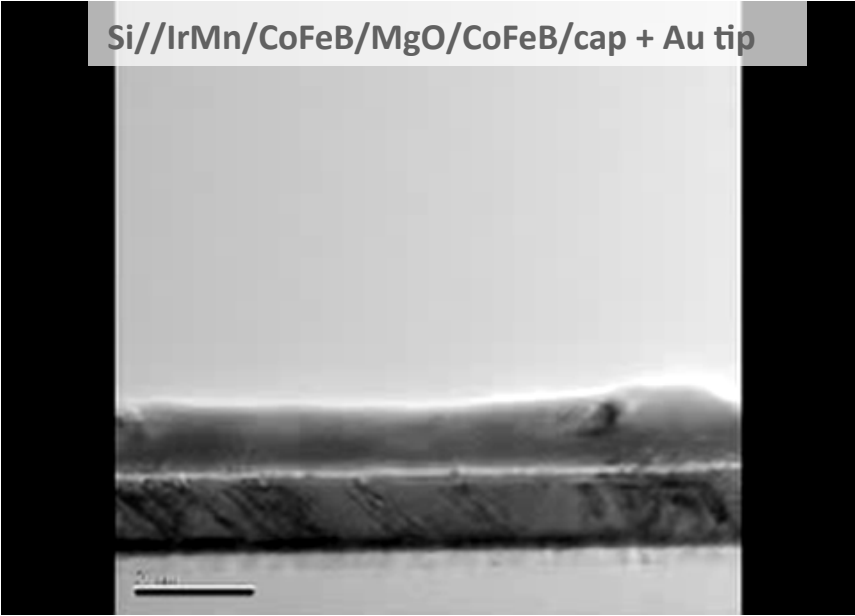


A.N. Chiamonti et al. *Ultramicrosc.*
108, 1529 (2008)

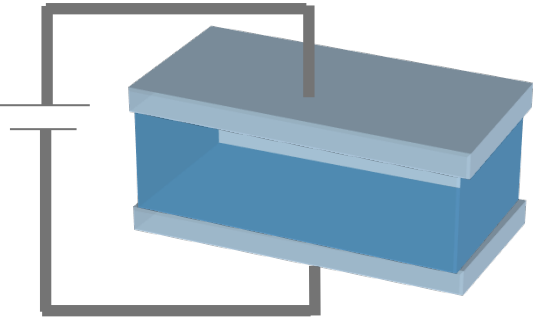


Hummingbird Nanobiasing holder

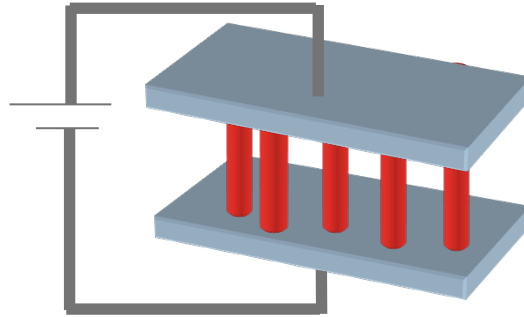
Si//IrMn/CoFeB/MgO/CoFeB/cap + Au tip



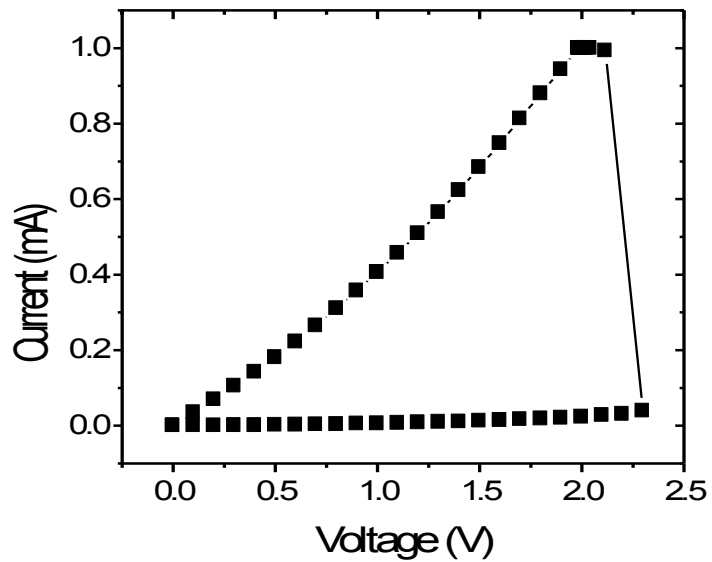
Electroforming NiO by Pt Migration



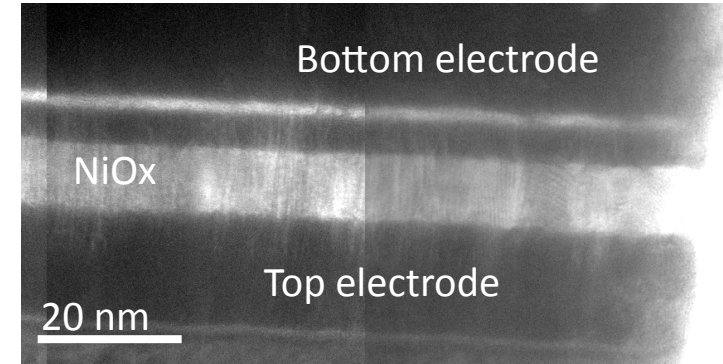
OFF state: high resistance
Uniform current flow



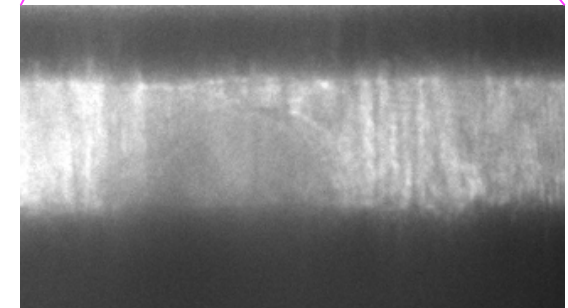
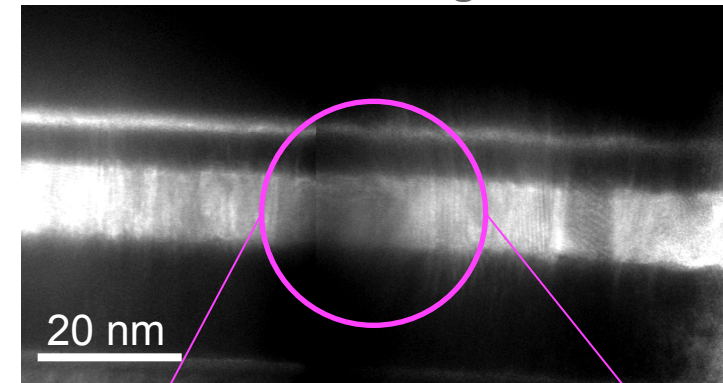
ON state: low resistance
Current flow along metallic filaments



Before forming



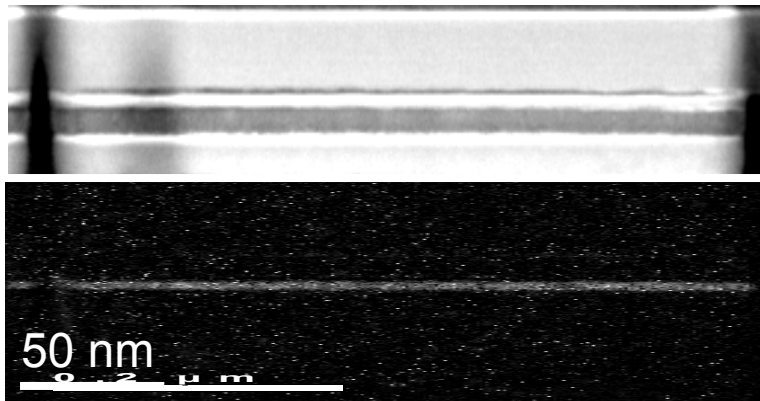
After forming



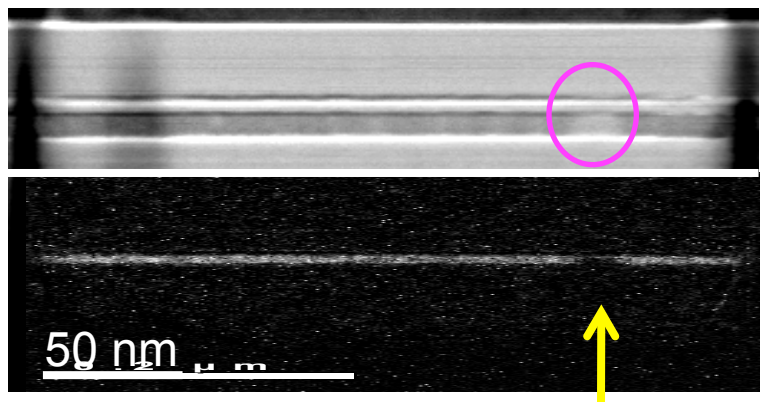
Ken D' Aquila and Yuzi Liu

Electroforming by Pt Migration

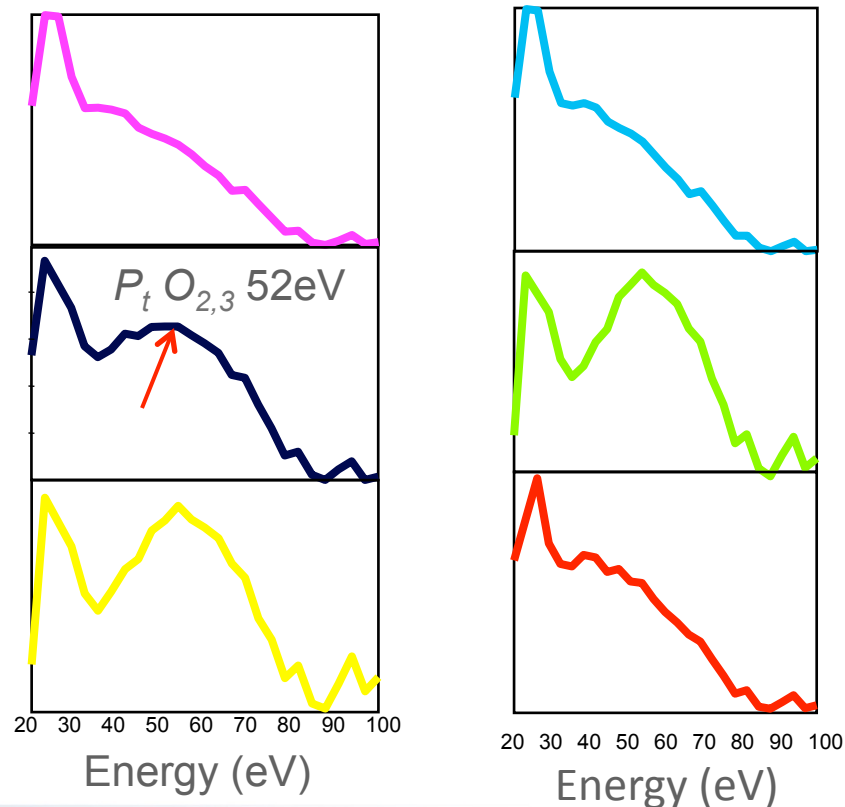
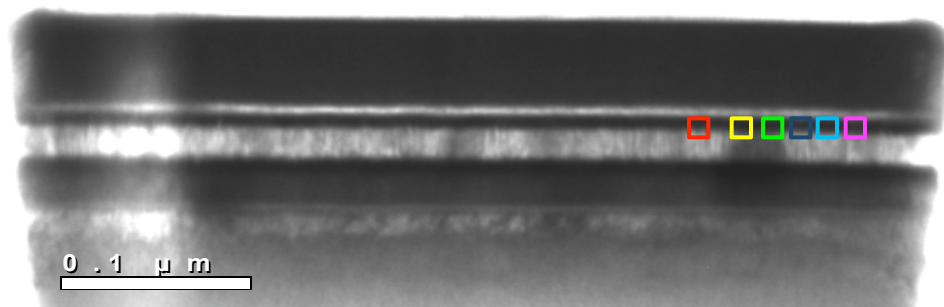
HAADF image (top) and Ni mapping (bottom) before electroforming



HAADF image (top) and Ni mapping (bottom) after electroforming



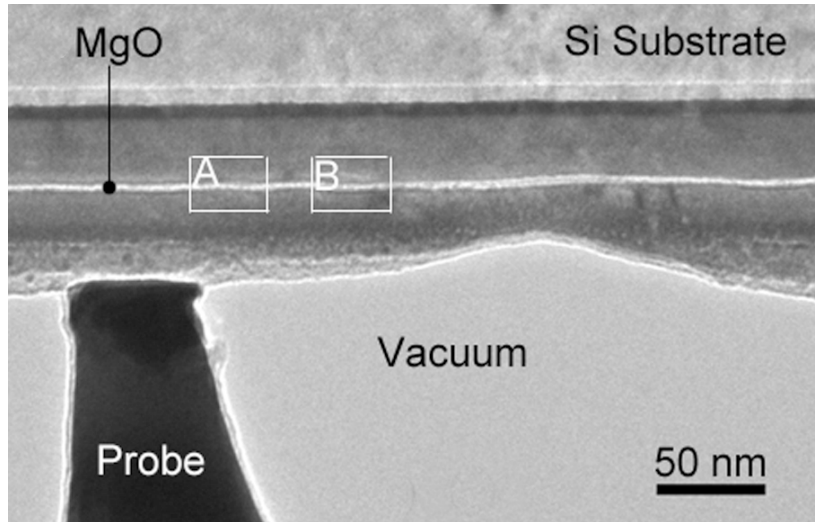
First spectrum image across Pt $O_{2,3}$ edge
(Stack from 20 eV–100 eV, step: 3 eV)



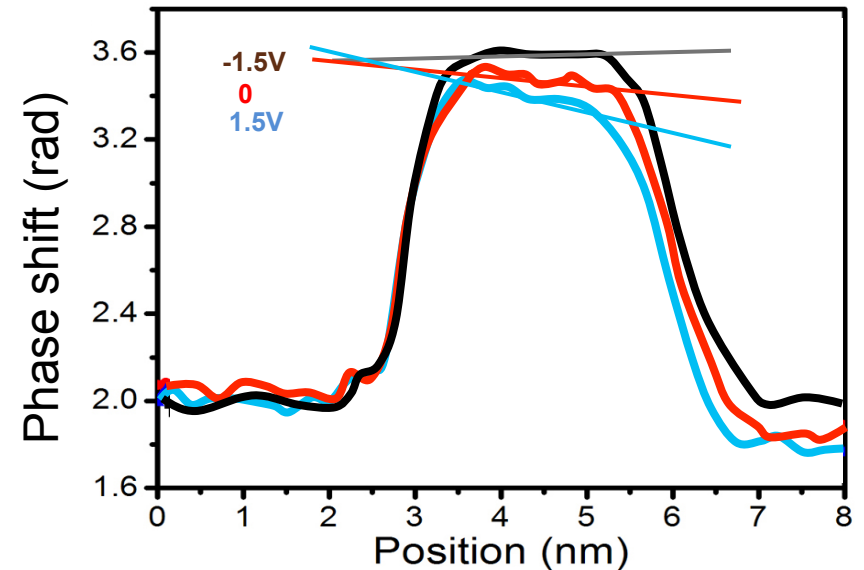
Ken D' Aquila and Yuzi Liu



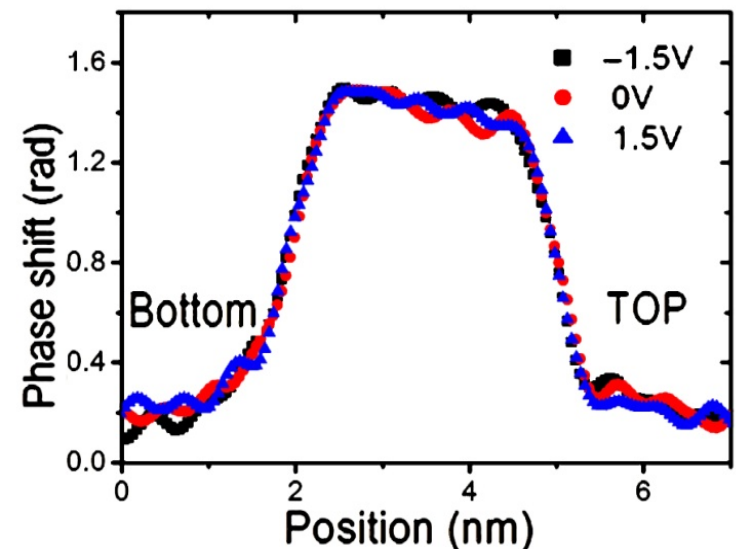
Effect of Probe Position on Barrier Shape



Under Au contact



Away from Au contact

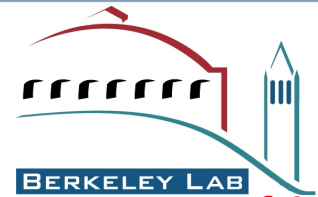


- Phase shift profile across the barrier is related to tunnel barrier shape & height
- The effective barrier width and asymmetry increase with increasing applied voltage from -1.5V to 1.5V
- “Control” curves recorded away from contact do not show this effect implying limited current spreading in electrode

Mechanical Testing



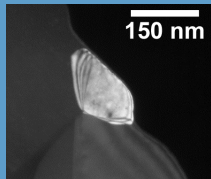
Advantages of *in situ* mechanical testing



Slide courtesy of Andy Minor, NCEM, LBL

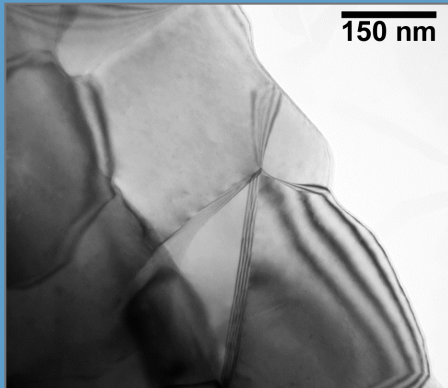
(1) Dynamics- when a before and after image just doesn't do

Before

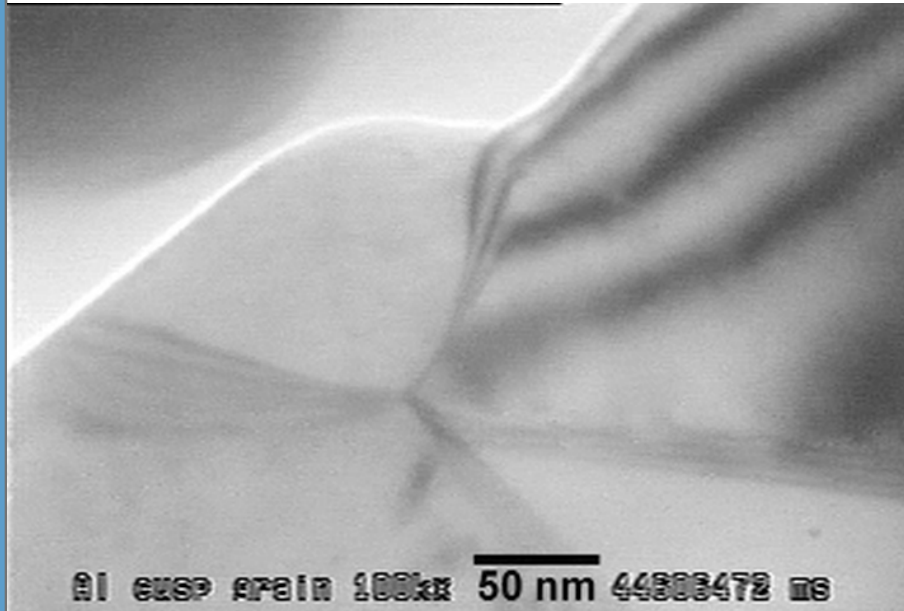


↑
g₂₀₀

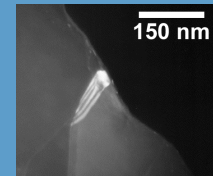
150 nm



During

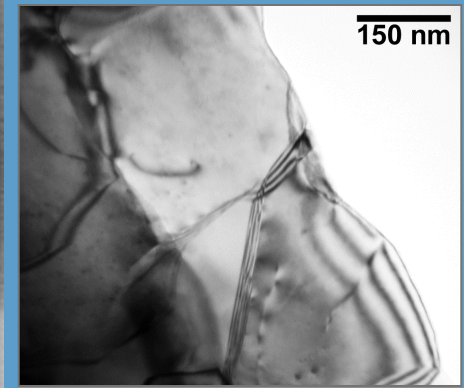


After



↑
g₂₀₀

150 nm



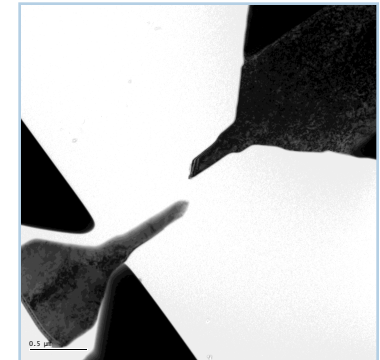
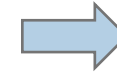
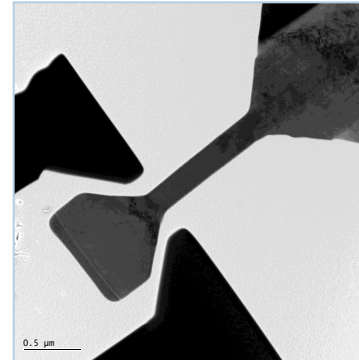
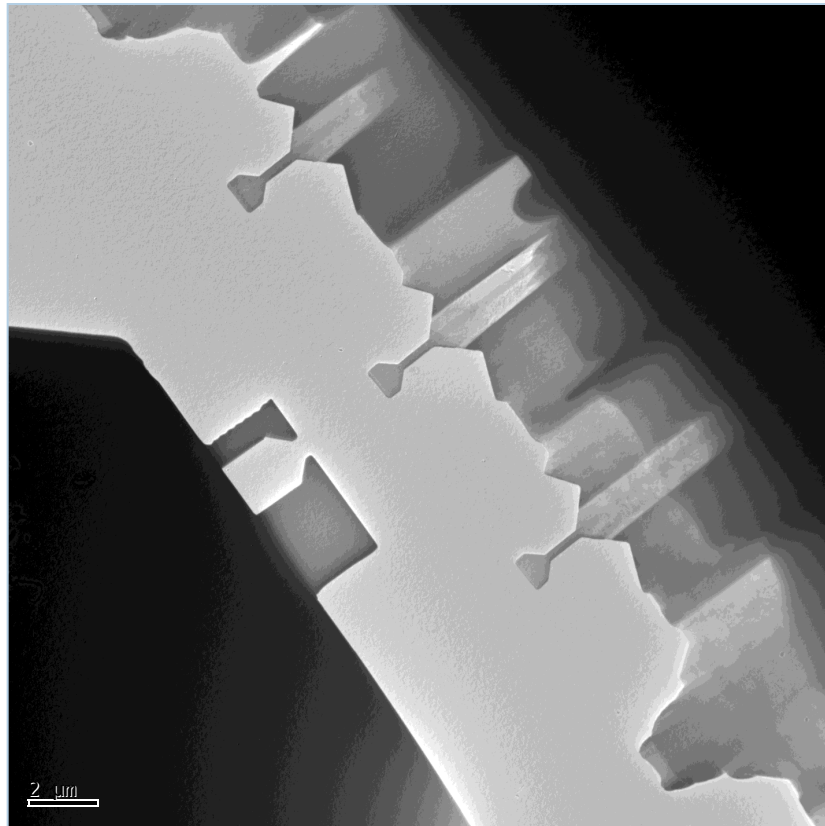
M. Jin, A. Minor, et al, Acta Mat 2004



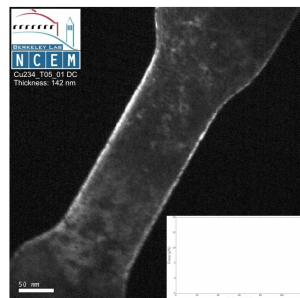
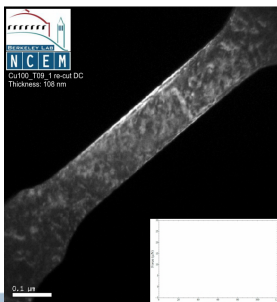
Quantitative in situ TEM tensile testing



Slide courtesy of Andy Minor, NCEM, LBL



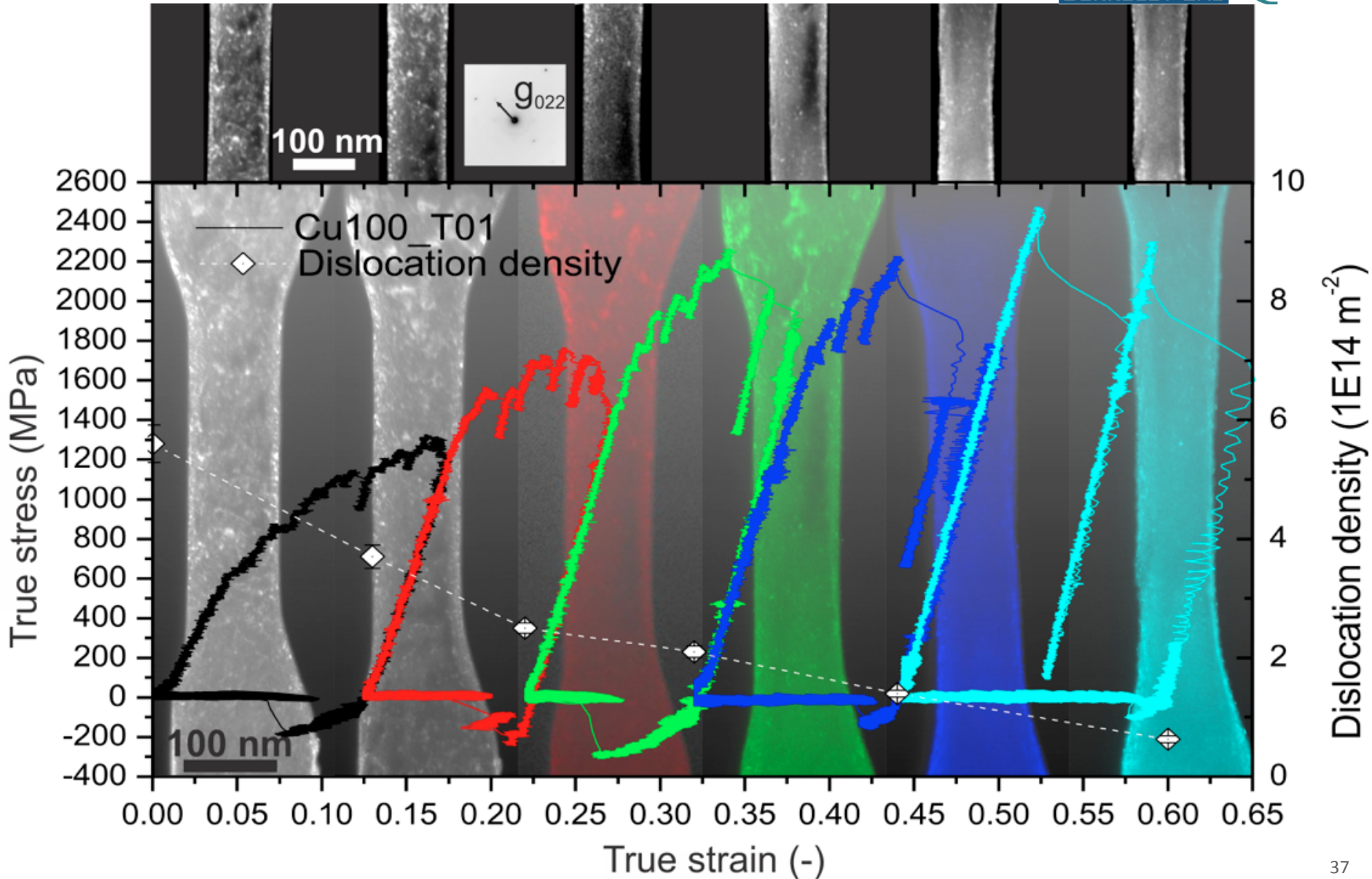
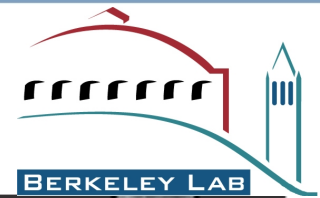
- FIB structuring of tensile samples allows for:
- Protective Pt deposition
 - Compensate for the taper
 - ($\sim 3^\circ$ or less, in one dimension only)
 - Vary surface to volume ratio (sheet vs. wire)
 - Well defined and variable gauge length



Typical dimensions:
Width: 200 nm
Length: 1000 nm
Thickness: 100 – 200 nm

Strength correlated to defects

Slide courtesy of Andy Minor, NCEM, LBL



Comparison: X-rays with (S)TEM

- TEM has higher spatial resolution (down to 0.1 nm or less with aberration correction)
-
- BUT: sample thickness is limited to 100-200 nm for most materials
 - Use of chromatic aberration correction greatly increases sample thickness that can be analyzed e.g. 1 μm for biological sample WITH high spatial resolution
- High energy electron beam (100-400 keV) can easily damage biological samples
 - X-rays also give rise to damage.... Would need to compare beam intensities
- FEGTEM in micro(nano)diffraction mode produces largest signal from smallest volume of material
 - Field-emission source is brighter than a synchrotron and the elastic scattering cross-section is very large
 - Probes down to ~ 0.1 nm can be achieved



CNM: a DOE user facility for nanoscience research



State-of-the-art scientific user facility at Argonne National Laboratory for the development and use of techniques for synthesis, fabrication, characterization and theory of materials at the nanoscale

Goals:

- A productive and satisfied user community
- High impact staff science
- Supporting the DOE BES mission in fundamental research and energy

<http://www.cnm.anl.gov>